Modelling the temperature envelope of concrete hydration in insulated forms at sub-zero temperatures

Jonathan Vänskä

Degree Thesis
Materials Processing Technology
2020

DEGREE THESIS	
Arcada	
Degree Programme:	Materials Processing Technology
Identification number:	21561
Author:	Jonathan Vänskä
Title:	Modelling the temperature envelope of concrete hydration in insulated forms at sub-zero temperatures
Supervisor (Arcada):	Rene Herrman
Commissioned by:	Nordicform Oy

Abstract:

The aim of the thesis is to demonstrate the viability of expanded polystyrene (EPS) insulated concrete form (ICF) and concrete construction in sub-zero [°C] environmental temperatures. The concrete core temperature was experimentally investigated at environmental temperatures between +10°C and -24°C. The thesis is conducted in co-operation with Nordicform Oy, and ICFs manufactured by Nudura. The scope of the thesis is to construct a thermodynamic model of the curing concrete, and to analyze the chemical and thermomechanical properties of construction grade concrete in ICFs. A predictive model of the concrete core curing conditions including an extrapolation of the strength from the time and temperature dependent maturity factor is created in Microsoft Excel. The model allows for prediction of critical environmental conditions that may result in incomplete curing. Heat flow analysis is used to mathematically model the cement hydration enthalpies and the flow of heat to the outside environment through the expanded polystyrene form. Time and temperature dependence of the hydration reactions of the main constituents of Portland cement and water are predicted and fit to experimental sensor data for a curing period of 28 days. Temperature data readings are collected once per hour with a measurement accuracy of ±1 [°C] and maturity-based strength is estimated to an accuracy of 0,1 [MPa]. The unit of study is one standard block of Nudura ICF and its concrete core. Temperature data for the inside of a concrete core at a construction site is collected using a Smartrock™ temperature and maturity sensor made by Giatec Scientific. The hydration reactions of alite ($3\,CaO \cdot SiO_2$), belite ($2\,CaO \cdot SiO_2$), tricalcium aluminate ($3\,CaO \cdot Al_2O_3$) and tetracalcium alumino ferrite ($4\,CaO \cdot Al_2O_3 \cdot Fe_2O_3$) and their interactions with water and gypsum ($CaSO\,4{\cdot}2H_2O$) are included. Interactions between the crystal growth of the various hydrate phases and their influence on compressive strength can be suggested. The equations for heat flow, and the Arrhenius and Avrami equations are used. The model is validated by predicting concrete temperatures at a secondary site. In the case study; data from the data indicate concrete core temperatures remain warm enough for concrete to reach its design strength within 28 days. In typical cold weather concrete construction, the EPS ICFs provide adequate insulation to allow for efficient curing. Extrapolating from the model, at environmental temperatures of below -20°C, concrete near an uninsulated, exposed surface such as: in a window opening or at the top of a wall section, may fall below a recommended limit of 4,4°C within the first 120 hours of curing. The design strength of concrete (30 [MPa]) is reached at 41 hours suggesting bulk concrete content is adequately insulated from the

elements. In conditions of below 20°C, additional insulation is required to protect open surfaces to ensure design strength is reached.	
Keywords:	Insulated Concrete Forms, Expanded Polystyrene (EPS), Portland cement, alite, belite
Number of pages:	62
Language:	English
Date of acceptance:	

CONTENTS

Figures

Tables

Equations

1 INTRODUCTION

1.1 Background

The composite material concrete is the most widely used artificial construction material in the world by a factor of two (Gagg, 2014). Structures constructed from concrete-like materials have been constructed since 1300 BC in the Middle East (Gromicko & Shepard, n.d.). Concrete consists of two main components: cement and aggregates. Cement consists of a varying blend of silicate and oxide minerals that act as a binder when hydrated in the presence of water. Aggregates typically consist of rock and/or sand particles. As aggregates are bound together by the hydration bonds of cement, concrete provides a durable, low-cost material useful in applications such as buildings, roads, and water transport systems. Some recognizable concrete structures include: The Colosseum of Rome, The CN Tower of Toronto, and the Opera House of Sydney.

Concrete construction in cold climates pose unique complications with structural strength. The causes of degradation of structural integrity include incomplete or uninitiated strength providing chemical reactions of cement, cracking caused by thermal

expansion and constriction, and complications due to under- and oversaturation possible through fluctuations of water content present in curing concrete (Vu, et al., 2015).

1.2 Aim of the study

The following thesis is an investigation of the thermal behavior of concrete curing in expanded polystyrene (EPS) insulated concrete forms (ICFs). The effect of temperature on the strength development of concrete in insulated forms has previously been outlined in a 2016 study in laboratory conditions (Won, et al., 2016). The aim of this study is to construct a predictive mathematical model of the inside concrete temperature and strength over time in a construction site setting. Based on the hydration enthalpies of the components of Portland cement, the total heat released is calculated. The ambient environmental temperatures are used to predict the heat lost from concrete. The objective of the study is to examine if the inside temperature of concrete can be predicted at a construction site using relatively few variables. The examined time period is 28 days of curing. Temperature data is collected from inside ICF walls at residential construction sites. This study aims to assess the effect of cold environmental temperatures on the integrity of the curing process and its effect on strength, as well as predict cases of failure during the curing process. Estimating the internal temperature of the concrete allows for the prediction of maturity without taking concrete temperature measurements. Using outside temperatures, time and the composition of concrete, the strength development of concrete structures can thus be estimated. This thesis is completed in co-operation with ICF products manufactured by Nudura Corporation based in Barrie, Ontario, Canada, and their Nordic distributor; Nordicform Oy.

1.3 Scope

The scope of the thesis is to construct a thermal model of the curing concrete and to analyze the chemical and thermomechanical properties and time-dependent changes of construction grade concrete. The model is fitted to measured temperatures. A mathematical model is built in Microsoft Excel to estimate the temperature of the inside of an ICF wall and is validated by applying the model to a secondary construction site and comparing the predicted temperature curve to the measured values. The parameters the prediction is

based on are the environmental temperature, the dimensions of the unit of study and the relevant specifications of the EPS and the concrete, such as the thermal conductivity and the specific heat capacity. The heat flow is predicted by calculating the amount of heat conducted out of the system as well as the heat released by the exothermic cement hydration reactions. The reactions of the main four constituents of cement are included in the model. A valid predictive model can be used to analyze how the expanded polystyrene insulation protects the curing concrete from thermomechanical damage or failure and the temperature profile can be compared to the strength profile. A central consideration is to examine whether curing concrete may be exposed to a temperature of 4,4 [°C] set by the Portland Cement Association as a critical limit (Klieger, 1958). The study will suggest the reliability of ICF construction in sub-zero temperatures and will create an outline for predicting material failures.

2 LITERATURE REVIEW

Existing literature is consulted to support the study and to provide knowledge of relevant topics. Topics of interest include the properties of the materials analyzed; primarily concrete and expanded polystyrene. The thermal, mechanical, and chemical properties and behaviors of the constituents of a constructed ICF wall system are studied. The hydration reactions of the main components of Portland Cement are studied and summarized. The properties and manufacturing and construction methods of expanded polystyrene and concrete are reviewed. Existing literature is consulted to find the relevant mathematical modelling methods necessary for the thesis. As an important consideration of the thesis is to analyze possible failures of ICF systems, different failure modes are studied and established regulations of concrete and ICF construction are reviewed.

2.1 Expanded Polystyrene

EPS is a closed cell rigid foam often used as insulation due to its low thermal conductivity. EPS is made of up to 98% air, acting as an efficient insulator with typical thermal conductivity values ranging from 0.036 – 0.046 [W/m·K] depending on the density, which varies between 10 and 30 [kg/m^3]. EPS consists of closed cell structures of 0,01-0,1mm in diameter (Yucel, et al., 2003). EPS is produced from styrene with pentane used as a

blowing agent. EPS can be blown directly into a mold. The styrene monomer is manufactured from petroleum products benzene (C_6H_6) and ethylene (C_2H_4). EPS is also a popular construction material as it is lightweight and relatively strong (Omnexus, n.d.). EPS can be fully recycled by compacting, melting, and remolding used polystyrene into new products (EPS Recycling International, 2019); it does not, however, decompose. The thermal conductivity may be increased due to manufacturing defects. EPS is a relatively low-cost material.

2.1.1 Insulated Concrete Forms

Insulated concrete form (ICF) is a construction system used to mould concrete into an insulated sandwich form. The form is typically composed of a polymer such as polystyrene or polyurethane. Modern ICF systems commonly have a built-in interlocking system allowing for stacking of blocks. Some ICF systems require an adhesive seal to be used to connect blocks. ICF construction is fast when compared to more traditional wall-building techniques such as wood framing or concrete block construction. The thermal conductivity of the insulated material is to be low. The total thermal insulation of a structure is provided by both the concrete and the sandwich insulation. ICF materials are typically efficient sound barriers, making them a desired construction method in loud environments such as cities. A commonly stated downside to ICF construction is their performance at low temperatures. The efficiency of the insulation in ICFs causes the outside temperature to have less effect on the inside temperatures; however, in cold climates, once the ICF and concrete are cooled, the low thermal conductivity may cause the wall to preserve a lower temperature once it has been reached. A commonly stated advantage of ICF construction is that the insulated sandwich panels help prevent low outside temperatures from causing expansion and compression cycles in freezing and thawing water content. In cold conditions, the activation energy of hydration reactions may not be exceeded. When the temperature in concrete falls below 5 [°C] incomplete hydration is expected.

2.2 Concrete

Concrete is a strong composite construction material made from cement and aggregates such as sand or gravel. Concrete is the most widely used construction material in the

world and its strength, hardness and durability. Concrete is often reinforced with steel to increase the tensile strength.

2.2.1 Cement Chemist Notation

For the purposes of this thesis, Cement Chemist Notation (CCN) is used. The relevant notations are outlined below.

Table 1: Cement chemist notation of concrete compounds

Name	Formula	CCN Name
Tricalcium silicate (alite)	$3\ CaO \cdot SiO_2$	C_3S
Dicalcium silicate (belite)	$2\ CaO \cdot SiO_2$	C_2S
Tricalcium aluminate (Aluminate)	$3\ CaO \cdot Al_2O_3$	C_3A
Tetracalcium alumino ferrite (Ferrite, brownmillerite)	$4\ CaO \cdot Al_2O_3 \cdot Fe_2O_3$	C_4AF
Calcium Silicate Hydrates	Various	C-S-H
Calcium hydroxide (port-landite)	$Ca(OH)_2$	CH
Calcium trisulfoaluminate hydrate (ettringite)	$Ca_6Al_2(SO_4)_3(OH)_{12} \cdot 26H_2O$	AFt
Aluminate ferrite mono-sulfate	$3CaO \cdot (Al,Fe)_2O_3 \cdot CaSO_4 \cdot nH_2O$	AFm
Dihydrogen monoxide (water)	H_2O	H
Calcium sulfate dihydrate (gypsum)	$CaSO_4 \cdot 2H_2O$	$C\underline{S}H_2$

2.2.2 Portland Cement

Cement is a hydraulic binding agent used in concrete, mortar and stucco. The total cement production in 2011 equaled 4,08 billion tons (Tradeship Publications Ltd, 2019). Ordinary Portland cement (OPC) is considered a synthetic inorganic polymer (Carraher, 2017). Portland cement is the most widely used type of cement used in construction, and will be the focus of this thesis. Other types of cement used in industry include Portland Pozzolana cement (PPC), quick-setting cement and high alumina cement.

Although the primary focus in this study is OPC, it is noteworthy to mention that PPC differs from OPC by the addition of pozzolana, which are silicate ash found naturally occurring in volcanic ash or as a by-product of industrial processes; the utilization of industrial waste products hence makes PPC an interesting alternative to OPC. PPC is often used in applications where a strong resistance to sulfate attack or other chemical deterioration is required, such as wastewater pipes or dams. Due to its fine particle size, PPC also gives a finer surface finish than OPC.

Portland cement consists of crushed limestone and clay minerals containing silica and aluminum. The production of Portland cement begins with the mining of the sedimentary rock limestone, mainly in open quarries (Minerals Education Coalition, 2021). Limestone is mainly composed of the most stable polymorph of Calcium Carbonate ($CaCO_3$) called calcite, however small amounts of aragonite or magnesium calcite may be present. Limestone is formed by the lithification of calcareous sediments primarily of organic origin (Haldar, 2014).

Quick-setting cement differs in that it includes a lower proportion of gypsum, which results in an initial rapid reaction of aluminate and ferrite content in the cement whereas high alumina cement contains a high alumina content (over 32%) and is used in applications where high heat resistance is required (Hanson Heidelberg Cement Group, 2020).

2.2.3 Cement manufacture

The raw materials are initially ground or crushed to pieces with an approximate diameter of 70mm (Rain Cement Limited, 2017). This may vary depending on the cement manufacturer. If larger particles are present, they are filtered out and re-processed. After initial

grinding, the particles are evaluated for their chemical composition to ensure homogeneity and limestone quality (Del Strother, 2019). A second, finer grinding is done with the objective of reducing calcium carbonate particle size to less than 125µm and a quartz particle size of less than 44µm to ensure complete calcination (Christensen & Smidth, 1979). Friction from grinding limestone produces heat, causing dehydration of the quarried limestone. Additional heat may be added to increase the efficiency of dehydration. Heat from the kiln is often recycled. The crushed particle blend is referred to as raw meal. The product after heating in a kiln is referred to as clinker.

Calcination is the first process in the precalciner kiln. The kiln consists of several reaction chambers, with a temperature increase in each consecutive step.

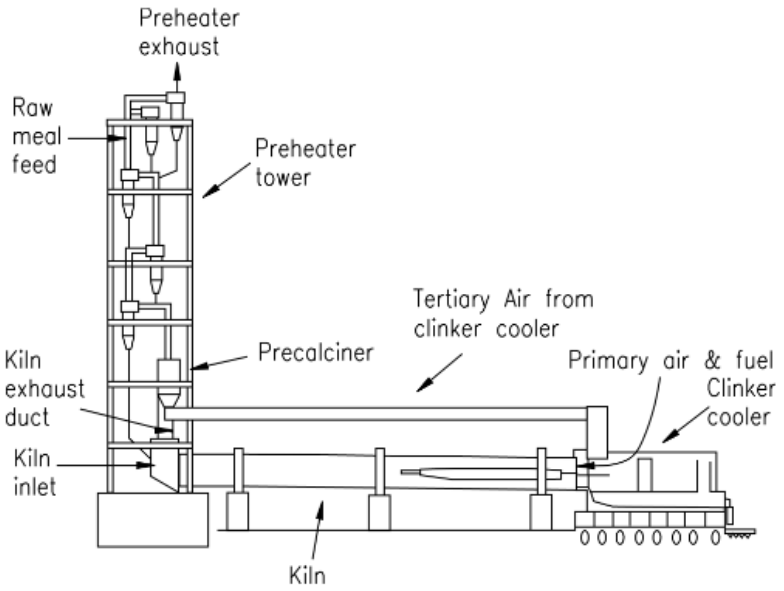

Figure 1: Precalciner Kiln ***(Renó, et al., 2017)***

Precalciner reactions:

1. Calcination usually refers to the process of thermal decomposition of calcium carbonate. The decarbonation reaction produces calcium oxide (CaO) also known as burnt lime and carbon dioxide (CO_2). More than half of the total carbon emissions from cement manufacture comes from the calcination process (Rodgers, 2018).

$$CaCO_3(s) \rightarrow CaO(s) + CO_2(g)$$

Reaction temperature: 800-900°C

2. In the second reaction chamber, the combination of burnt lime (CaO) and quartz (SiO_2) produces belite ($(CaO)_2 \cdot SiO_2$). Some belite remains in the complete clinker product and contributes to the late strength of OPC (Odler, 2003).

$$CaO(s) + SiO_2(s) \rightarrow ((CaO)_2 \cdot SiO_2)(s)$$

Reaction temperature: 800-900°C

3. Aluminum and iron oxides melt rapidly creating a liquid flux, that allows for the transport of lime and quartz. When the volume of liquid reaches between 15 and 25%, alite formation begins (Glasser, 2003, p. 233).

$$Al_2O_3(s) + Fe_2O_3(s) \rightarrow Al_2O_3(l) + Fe_2O_3(l)$$

Reaction temperature = 1300-1400°C

4. Dissolved free lime, belite and quartz are transported through the molten flux and react to form alite (Glasser, 2003, pp. 233-234).

$$CaO(s) + ((CaO)_2 \cdot SiO_2)(s) \rightarrow ((CaO)_3 \cdot SiO_2)(s)$$

Reaction temperature over 1300°C

5. After alite formation, the clinker enters a rapid cooling phase. It is important to cool the clinker mix rapidly, to prevent alite from reducing to belite (Del Strother, 2019, pp. 49-50). Aluminate and ferrite are formed as the temperature is reduced. They do not contribute significantly to the strength of OPC, and they hydrate rapidly when in contact with water.

$$4CaO + Al_2O_3 + Fe_2O_3 \rightarrow (CaO)_4 \cdot Al_2O_3 \cdot Fe_2O_3$$

And

$$3CaO + Al_2O_3 \rightarrow (CaO)_3 \cdot Al_2O_3$$

The ready cement is a mix of the different calcination products. Different types of cements are created by mixing different ratios of the four main components (C3S, C2S, C3A, C4AF).

For concretes requiring special characteristics such as sulfate resistance or resistance to humidity, special additives such as MgO may be added.

2.3 Concrete Curing

Water is added to anhydrous concrete to initiate the curing process. In a construction setting water is added at the concrete plant before the concrete is delivered in a truck mixer. A rotating blade continually mixes the concrete to prevent premature hardening in the truck mixer. The main reaction in concrete curing is the hydration reaction of calcium silicates. Alite and belite are hydrated to produce calcium hydroxide (CaOH) and Calcium Silicate Hydrates (C-S-H). Factors that impact the rate of hardening include the alite to belite ratio, aluminate and gypsum content, fineness, water to solid (w/s) ratio, and initial temperature.

High early strength cements contain higher concentrations of alite and aluminate (Dunuweera & Rajapakse, 2018). The alite hydration reaction is the dominant strength - providing reaction. Some cement manufacturers may increase the alite concentration for faster setting. Increased aluminate concentration will release heat, providing free energy to accelerate the alite hydration process. Gypsum ($CaSO_4 \cdot 2H_2O$) content is increased in high early strength cements to prevent premature “flash” setting, which impacts strength development and workability.

Rapid hardening of concrete can be improved by decreasing the concentration and particle size of aggregates, and finer grinding (increasing surface area) of the cement clinker. The fineness of the cement grind can be expressed in terms of specific surface area (m^2/g). The most common method of determining the specific surface area (SSA) is the Blaine Air Permeability test. The standard test procedure is described in EN 196-6 as well in ASTM and ISO standards, and models the volume of air flow through a sample as a function of time. Typical fineness for Portland Cements is between 3000 and 4500 cm^2/g with rapid hardening cements having a higher SSA than ordinary and low heat cements.

Fineness is the main difference between ASTM Type I (ordinary) and ASTM Type III (high early strength) cements.

A typical heat of hydration-graph is shown below. The hydration profile showing all hydration heat releases should be conducted in a calorimeter study, as environmental influences can cause hydration peaks to be less visible in data. A high sampling rate (such as 15 minutes) can help visualize separate exothermic hydration periods more accurately. A general representation of the heat of hydration of Portland cement is shown below.

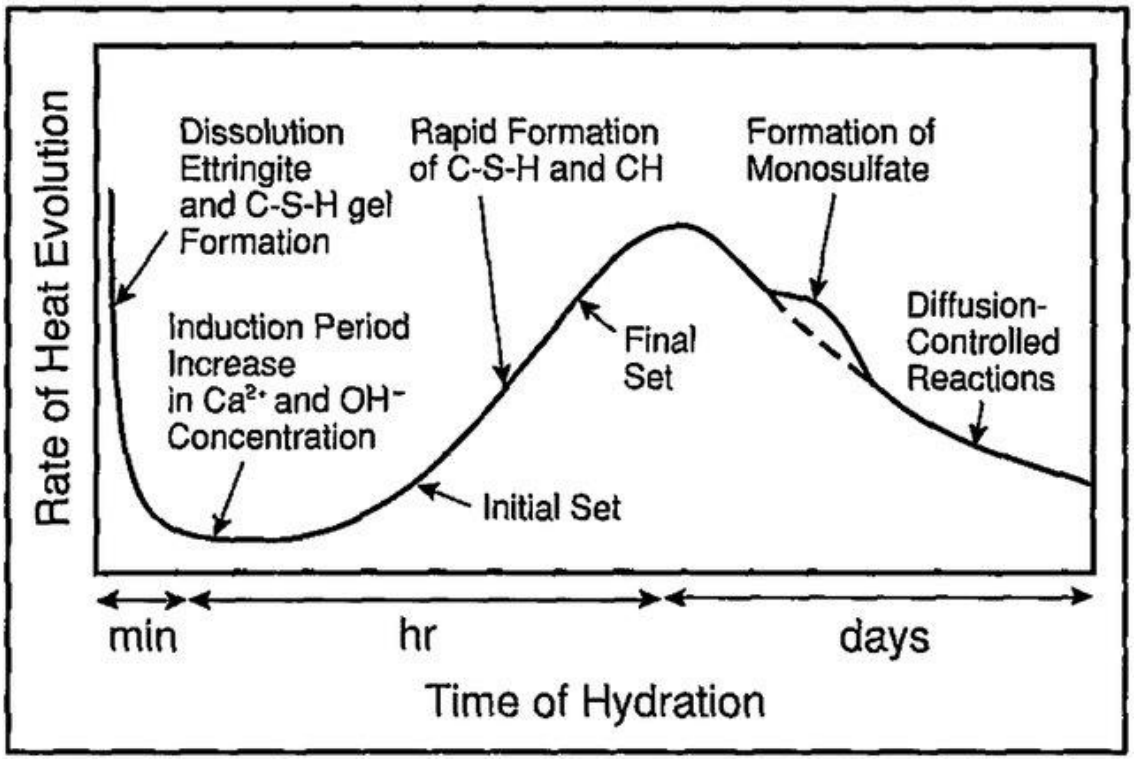

Figure 2: Heat of hydration (Salami, 2014)

The complete hydration enthalpies are listed in the table below. The complete hydration enthalpies can - in association with reaction rates and completion percentages - be used to predict complete hydration heats as a function of time. The volumetric changes in concrete may also be modelled as a function of the water content and the percent completion of the hydration reactions. Concrete mixes with a high water to solid-ratio are most susceptible to shrinkage (Nmai, et al., 2018). It should be noted that the complete hydration heats listed below are from calorimeter studies and complete hydration is not always reached in construction processes.

Table 2: Complete hydration enthalpies of Portland cement constituents (Beaudoin & Odler, 2019)

Reactants	Products	Enthalpy J/g
C_3S+H	C-S-H+CH	520
βC_2S+H	C-S-H+CH	260
$C_3A+C\underline{S}H_2+H$	AFt	1670
$C_3A+AFt+H$	AFm	1140
$C_4AF+CH+H$	$C_3(A,F)H_6$	420

The structure of hydrated cement includes hydrated crystals of the main constituent elements. The various hydrates provide strength to concrete. The elastic moduli (Young's modulus) of some of the main products are outlined below.

Table 3: Elastic modulus of concrete constituents (Termkhajornkit, Vu, Barbarulo, Daronnat, & Chanvillard, 2014) (Manzano, Dolado, & Ayuela, 2009) (Pellenq & Van Damme, 2004)

Phase	Young's modulus [GPa]
C-S-H	57,1
Ettringite	22,4
AFm	42,3
CH	42,3
C_2S	130
C_3S	135

The main strength-providing components are the hydration products of alite (C_3S) and belite (C_2S); Calcium-Silicate-Hydrates (C-S-H) and portlandite (CH). Crystalline globular C-S-H molecules will bond with other hydrate species as the hydration approaches completion, and void content is eliminated. AFm provides early strength to concrete,

however due to its needle-like structure, its bonds with C-S-H are relatively weak. Increasing sulfate content has a negative effect on the late strength, with the optimum amount typically listed as between 2 and 3% (Paine, 2019, pp. 303-307)

A representation of the shapes of some of the main clinker phases are shown in the image below.

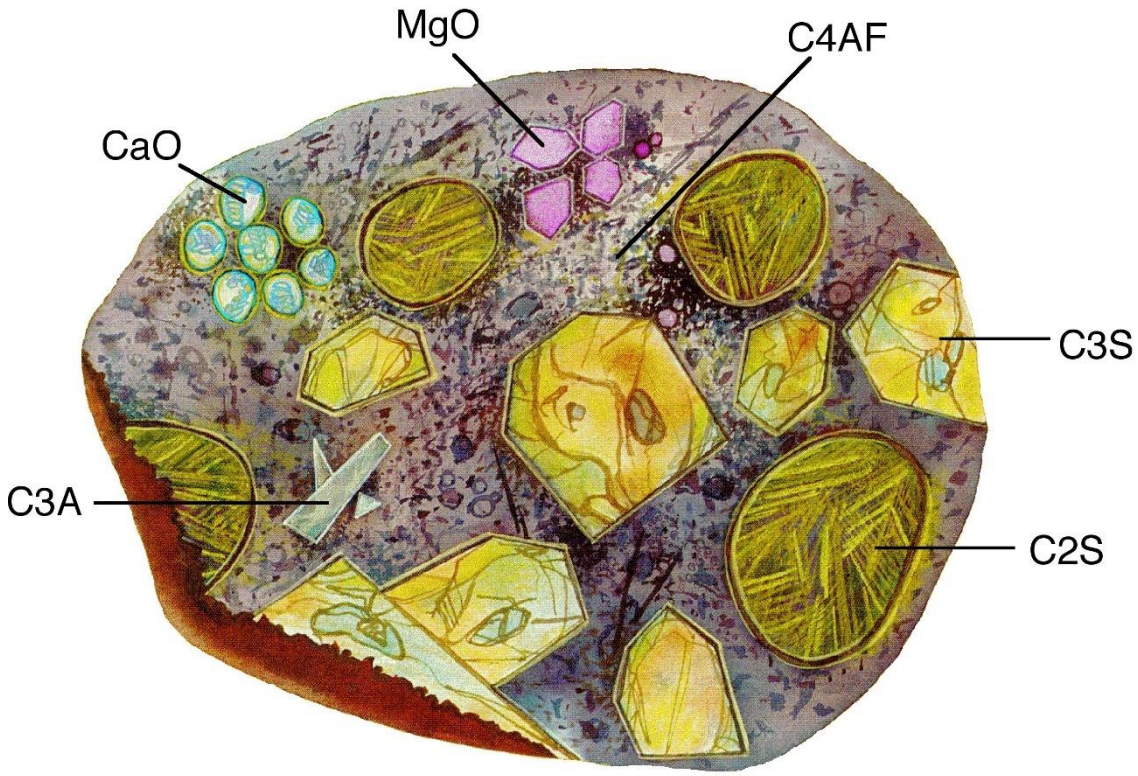

Figure 3: Clinker phase shapes (Barron, 2010)

2.3.1 Alite hydration

The hydration and nucleation of alite is the primary chemical reaction giving concrete its early strength. Immediately after mixing, there is an induction period where the reaction happens slowly. The cause of the induction period is not fully known (Bergold, et al., 2015). The hydration products are calcium hydroxide (portlandite) and stoichiometrically non-homogenous molecules collectively referred to as Calcium-Silicate-Hydrates (C-S-H). The alite hydration reaction is characterized by subdividing it into pre-induction,

induction, and post-induction periods. The different reaction stages release varying amounts of energy and create different hydration products.

2.3.1.1 Pre-induction period

The pre-induction is initiated upon contact of the anhydrous clinker with water. An initial release of heat is detectable. Although there is no consensus on the exact reaction kinetics of the pre-induction and induction periods, it is hypothesized that an initial protective, unreactive hydrate layer forms around the alite. This is, however, difficult quantify due to calorimeter inertia and initial heat from friction (Nicoleaua & A., 2016). The dissolution of alite progresses once the initial C-S-H layer becomes more permeable.

2.3.1.2 Induction period

During the induction period there is little reactivity or heat released. This may be due to undersaturation of alite and the protective layer preventing alite from dissolving into its constituents (calcium and silicates). The protective layer theory predicts the formation of a metastable semicrystalline hydrate structure around alite, which eventually transforms into a more stable and more permeable form (Gartner & Jennings, 1987). Nuclear Magnetic Resonance (NMR) studies confirm the formation of monomeric silicate hydrates during the early induction period. In a 2016 NMR study, silicate bonding and polymerization is analyzed with strong monomeric silicate (silanol) presence observed during the induction period. The resonance signal indicating presence of silanol is due to the hydroxylation of the surface of alite. Dimeric silicate formation is observed at the end of the induction period (Pustovgar, et al., 2016). It is hypothesized that the induction period is a time of slow reactions with both nucleation and hydration reactions happening. "Up until the precipitation of portlandite, the rate controlling mechanism is the solution-controlled dissolution (SCD) of alite (Kumara, et al., 2012)."

$$Ca_3SiO_5 + 3H_2O \rightarrow 3Ca^+ + 4(OH^-) + H_2SiO_4^{2-}$$

The degree of undersaturation determines the rate of dissolution. As the water becomes saturated with the calcium and silicate ions, the rate of dissolution slows.

2.3.1.3 Acceleration period

The acceleration period begins with a rapid increase in the hydration rate of alite and is initiated as the solution concentration of dissolved calcium and silicate ions increases.

The acceleration period is highly exothermic, and in an insulated system, the free energy further increases the reaction rate. Formation of oligomeric C-S-H precipitates from the dissolved calcium and silicates begins as dimeric C-S-H species polymerize. Typically, pentameric and octameric C-S-H forms are observed. Monomeric and dimeric species persist after 1,5 months of hydration (Pustovgar, et al., 2016). Scanning Electron Microscope (SEM) studies further confirm the existence of a layer of C-S-H forming around alite, acting as a diffusion barrier (Gartner, et al., 2002, pp. 70-72).

During the acceleration period, the concentration of free Ca^{+} in solution can be observed to decrease rapidly (Paulini, 1990). Free dissolved calcium hydrates to form portlandite ($Ca(OH)_2$) (Beaudoin & Odler, 2019).

The acceleration stage of alite hydration can be estimated with the equation below.

$$3Ca_3SiO_5 + 6H_2O \rightarrow (3CaO \cdot 2SiO_2 \cdot 3H_2O) + 3Ca(OH)_2$$

2.3.1.4 Deceleration period

The reaction rate of alite hydration begins to decrease as calcium ions in solution are reacted and polymeric C-S-H species and CS fill voids. Diffusion through the C-S-H barrier of calcium or silicates is slowed due to the increasing size and overlapping of hydrates. Porosity is much reduced. During this period, the internal temperature of concrete will begin to approach the temperature of the external environment, as less heat is generated.

C-S-H products formed during the acceleration and deceleration stages include complete crystalline hydration products; tobermorite and jennite. Tobermorite ($Ca_4Si_6O_{17}(H_2O)_2 \cdot (Ca \cdot 3H_2O)$) consists of a central layer consisting of calcium oxides sandwiched between parallel silicate chains. Every third silicate tetrahedra is kinked. Between chains of tobermorite there is an intermediate water and Ca^{+}, which neutralizes the electronegativity of the C-S-H chains.

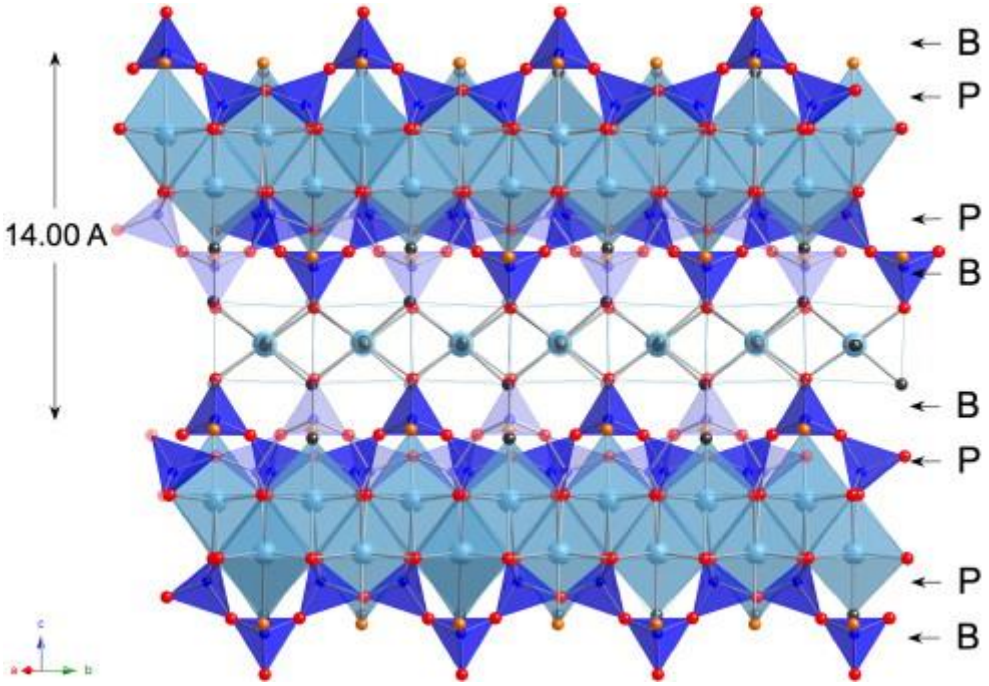

Figure 4: Tobermorite structure (Richardson, 2008, p. 144)

The other important C-S-H structure is jennite ($Ca_9Si_6O_{18}(OH)_6 \cdot 8H2O$) which is similar in structure to tobermorite, but half of the central layer oxygen atoms are replaced by hydroxyl groups (Richardson, 2008, p. 144).

2.3.2 Belite Hydration

At the end of the alite hydration acceleration period (100+ hours), the hydration rate of belite begins to increase gradually. This growth in belite hydration will continue for 1000+ hours, giving the concrete its late strength. Similarly to alite hydration, an acceleration and deceleration period is observed in isothermal calorimetry studies

The hydration products of belite are (C-S-H) species and CH. β-belite is the only metastable polymorph at room temperature. Other belite polymorphs are active at high temperatures and are relevant in clinker manufacture (Beaudoin & Odler, 2019). The completion of the β-belite hydration is expected to reach approximately 40% after 1000 hours of curing (Qi, et al., 2021).

2.3.3 Aluminate Hydration

The aluminate hydration reaction happens very rapidly. To prevent rapid (flash) of cement, sulfates, most commonly gypsum is added (Odler, 2003). In the absence of gypsum or other sulfates between 70-90% is reacted within the first 24 hours of curing. The exothermicity of the initial gypsum and aluminate reaction is low. The initial reaction of aluminate and gypsum to form ettringite can be summarized as:

$$Ca_3Al_2O_6 + (3CaSO_4 \cdot 2H_2O) + 26H_2O \rightarrow (3CaO \cdot Al_2O_3 \cdot 3CaSO_4 \cdot 32H_2O)$$

(Portland Cement Association, 2001)

Ettringite forms a barrier around anhydrous aluminate preventing it from a rapid hydration reaction. Ettringite is the most common species of the aluminate, ferric oxide trisulfates (AFt). At high calcium sulfate concentrations, some ettringite may remain in the final concrete. If the calcium sulfate concentration is low, ettringite will reform to calcium aluminate monosulfate, a type of aluminate: ferric oxide monosulfate (AFm). Ettringite forms needle-like crystalline structures are shown in an SEM image below.

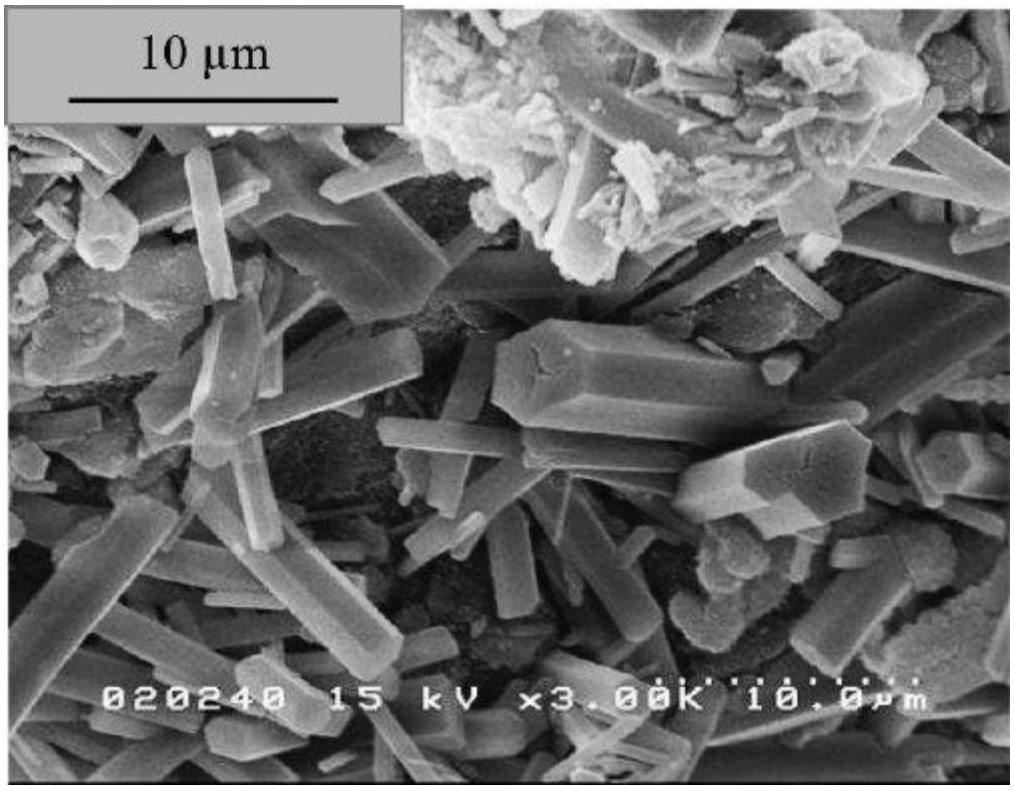

Figure 5: Ettringite crystals (Jewell, et al., 2015)

As the free sulfur ions in the solution are consumed, ettrengite begins to react with C_3A. This reaction is very rapid and exothermic. As the initial ettrengite layer is reacted, the formation of C_4AH_{19}, a hexagonal calcium aluminate hydrate, begins. The hexagonal hydrate acts as a diffusion barrier around aluminate, slowing hydration reactions. This initial hydrate is reduced to C_3AH_6, a cubic form, which is more permeable to water (Beaudoin & Odler, 2019). The reaction product is calcium aluminate monosulfate ($3CaO{\cdot}Al_2O_3{\cdot}CaSO_4{\cdot}12H_2O$), which is an analogue of the mineral kuzelite. Afm remains in the final hydrated concrete. The structure of AFm consists of a sulfate ion and water interlayer sandwiched between $Ca_3Al(OH)_6$ layers. The metastructure of kuzelite is hexagonal in its crystalline form (Beaudoin & Odler, 2019, pp. 177-178) (Berman & Newman, 1963). The reaction between ettrengite and tricalcium silicate to form a hydrated calcium aluminate monosulfate can be summarized as:

$$(3CaO \cdot Al_2O_3 \cdot 6H_2O) + (CaSO_4 \cdot 2H_2O) + 4H_2O \rightarrow (3CaO \cdot Al_2O_3 \cdot CaSO_4 \cdot 12H_2O)$$

Although aluminate hydration to Aft and AFm, contributes little to the compressive strength of concrete, the heat released by the rapid reaction, increases the rate of C_3S and C_2S hydration.

2.3.4 Ferrite Hydration

Calcium aluminoferrite species found in cement vary in composition from calcium ferrite ($2CaO{\cdot}Fe_2O_3$) to calcium aluminoferrite ($6CaO{\cdot}2Al_2O_3{\cdot}Fe_2O_3$) with various possible ratios of aluminum and iron content. The ratio of aluminum to iron in these compounds influences the reaction rate with higher aluminum content reactants hydrating faster. Species with high aluminum content have higher specific surface area (Carlson, 1964). The hydration of calcium aluminoferrites resembles the hydration mechanisms of calcium aluminates with CaO, Al_2O_3, and Fe_2O_3 dissolving into solution and subsequently combining to hydrated forms. In gypsum containing reactions, aluminate AFts form first, with subsequent formation of iron containing hydrates.

Some aluminum in the structure is substituted for iron in the lattice structure. Iron (Fe) ettringite takes the form ($(Ca_6[Fe(OH)_6]_2(SO_4)_3 \cdot 26H_2O$) (Möschner, et al., 2008). The

maximum value of substitution is not fully defined in literature, however values of between 9 to 21,5% are suggested

2.4 Concrete failure modes

Multiple failures in concrete construction are possible. These are caused by insufficient thermal or mechanical resistance. Incomplete curing is a major cause of structural failure of concrete structures. Other causes of concrete failure may be attributed to factors such as design errors or errors in construction. In cold climates a major cause of structural deterioration is freeze-thaw cycles that concrete is subjected to.

2.4.1 Thermal damage

A major cause of concrete failure is incomplete curing due to cold temperatures. Concrete is most susceptible to damage during first 25 hours of curing, when the free water content is high. The susceptibility of concrete to thermal damage is related to the degree of water saturation, as the water concentration decreases, the potential for damage decreases. In cold temperature pours, the water to solid (w/s) content should be kept as low as possible, while providing an adequate level for proper curing. Initial freezing of saturated concrete causes the concrete to be permanently more susceptible to freeze-thaw damage.

The expansion and shrinkage of water in pores can in some cases exceed the tensile strength of the concrete and cause cracking. Repeated freeze-thaw cycles cause fractures to form in concrete, which significantly affect the strength. Frost damage will occur during concrete curing if the concrete is oversaturated and the temperature fluctuates, causing freeze-thaw cycles of the water content present. The frost resistance of concrete is classified according to the number of freeze-thaw cycles it is subjected to without significant deterioration. Sections of a material where a large thermal gradient is present are especially susceptible to thermal shock damage.

Concrete may still hydrate at temperatures of -10°C, due to the water content being unable to freeze, in small, high-pressure capillary pores. According to the American Concrete Institute (ACI), the saturation degree of concrete is considered secure for one freeze-thaw

cycle when the compressive strength reaches 2,5MPa. During the first 24 hours of curing, temperatures below 0°C in concrete will cause permanent damage to the strength, as the large volume of water present causes expansion. ACI considers conditions of outside temperature of below 5°C for 3 days or 10°C or less for 24 hours as a general guideline to take measures in heating or insulating the concrete (Neville, 2011) (Portland Cement Association, 2019). Concrete must sustain its designed compressive strength.

2.5 Standards and codes

The important standards to be met by the EPS and concrete are included in national building codes as well as the standards outlined for the ICF. The compressive strength of concrete to be used in ICF construction is outlined in the European Technical Assessment (ETA) of Nudura ICFs, as C20 or higher depending on the application. The design strength must be reached within 28 days. The thermal conductivity of Nudura EPS panels (permanent insulating formwork) is listed by the ETA as 0,036 [$\frac{W}{m \times K}$].

2.5.1 EN 197-1

The European standard for construction cement and concrete is created by the European Committee of Standardization. The applicable code for construction in Finland is the EN 197-1 document.

“Portland cement clinker is a hydraulic material which shall consist of at least two-thirds by mass of calcium silicates (3CaO · SiO2 and 2CaO · SiO2), the remainder consisting of aluminium and iron containing clinker phases and other compounds. The ratio by mass (CaO)/(SiO2) shall be not less than 2,0. The content of magnesium oxide (MgO) shall not exceed 5,0 % by mass.” (British Standards Institution, 2011). The content of (MgO) is to be kept low due to its “long-term dimensional instability” (Nobre, et al., 2020).

The standard also outlines that the marketed strength of the concrete must be in accordance with a strength test complete at seven days for the early strength and the specific class strength at 28 days.

2.5.2 Concrete classes

Concrete is classified according to several parameters including compressive strength classes, exposure classes including deterioration due to humidity, freezing or corrosion due to sea water. It is important to select the correct concrete for the application and the location of construction.

2.5.2.1 Strength classes

Concrete is classified according to its compressive strength. These classes are outlined as, for example, C25/30. When in standard notation, the 25 indicates a characteristic cylindrical compressive strength of 25MPa and the 30 is the characteristic cube compressive strength at 28 days of curing. The testing procedures are outlined in EN 197-1. The cylindrical sample is tested with a diameter of 150mm and a thickness of 300mm. The cubic sample is to have dimensions of 150mm by 150mm (Harrison & O, 2007).

2.5.2.2 Consistency classes

Another characteristic important to concrete curing is the consistence (workability or slump). This characteristic defines how easily the concrete will flow. Three main classes are outlined as S1, S2 and S3. S1 is considered dry mix and is used when high flow is undesirable. S2 is considered moist mix and is used in simple footings and is the most widely used consistence. S3 is considered wet mix and is used when a deep trench is filled. S3 has a low viscosity and will fill deep openings evenly.

2.5.2.3 Exposure classes

Exposure classes define requirements of concrete under environmental conditions. The ones that are applicable in this study are the XF classes, which describe freeze load conditions, and XC classes, which describe effects of carbonation.

In Finland thermal expansion and constriction can have a large effect on concrete, so the appropriate grade of concrete must be used. The XF classes describe the conditions of water saturation and degree of environmental thermal changes (Harrison & O, 2007). Classes XF1 and XF2 describe low water saturation conditions with and without de-icing agents. Classes XF3 and XF4 describe high water saturation conditions with and without de-icing agents.

The XC classes describe the degree of environmental humidity and air that the concrete is subject to. The classes range from XC 1 to XC 4 with each describing increasing deterioration due to carbonation (Harrison & O, 2007).

3 METHOD

To analyze the thermal reactions happening in the constructed wall, a sensor is placed in the ICF structure to measure the internal temperature of concrete after pouring and to estimate the strength using a calculation of maturity. The sensor used is the SmartRock 2 made by Giatec Scientific. A predictive mathematical model of the temperature is fit to the measured values. The variables used in the model are the dimensions of the EPS block and the concrete core, the known environmental temperature and literature values of the hydration enthalpies of alite, belite, aluminate, ferrite as well as their proportions in the cement mix.

The unit of study is one standard block of Nudura EPS foam and its concrete core. The volume of reinforcement steel is neglected.

3.1 Mathematical theory

Multiple mathematical functions are needed to fully describe the system. In addition to using theoretical mathematical equations describing reaction rates and heat flow, experimental observations are used to improve model parameters.

The factors included in the enthalpy calculations are the temperature dependent reaction rate, the completion ratio, and the heat flow in and out of the concrete. The reaction and completion rates are calculated for each hydration reaction. The heat flow is calculated for one hour time intervals and the state of the system is assumed to be steady within each interval.

3.1.1 Arrhenius equation

The Arrhenius equation is used to calculate the temperature dependent reaction rate. Values of "k" are found in existing literature for various temperatures. Existing studies, where the values of "k" are found are calorimetric studies of the isolated components of cement (alite, belite, aluminate/ferrite) hydrated in known temperature conditions. The relation of temperature and reaction rate from existing studies are plotted and the remaining terms; the pre-exponential factor "A_1" and the apparent activation energy "E_a" are found.

For each hydration reaction the reaction rate is found for each time step (one hour) and is based on the previous value of the temperature.

$$k = A_1 e^{(\frac{-E_a}{RT})}$$

Equation 1: Arrhenius equation (Mortimer & Taylor, 2002, p. 65)

(1)

k = reaction rate (frequency of collisions resulting in a reaction) $[\frac{1}{h}]$

$\mathrm{R} = \text{Universal gas constant } (8{,}314\ \left[\frac{\mathrm{J}}{\mathrm{mol} \times \mathrm{K}}\right]$

A_1 = pre-exponential factor [unitless]

3.1.1.1 Activation energy from Arrhenius plot

The activation energy extracted from the Arrhenius plot is used as a factor in determining the temperature dependence of reactions.

$$E_a = R \times slope \quad (2)$$

Equation 2: Activation energy from Arrhenius plot

The slope is graphed and can be described as

$$slope = -(T \times \ln\left(\frac{k}{A_1}\right)) \quad (3)$$

Equation 3: Slope of Arrhenius plot

3.1.1.2 Pre-exponential factor from Arrhenius plot

To find the pre-exponential factor of the Arrhenius equation, the equation may be rearranged to find "A_1"; when "k", "E_a", and "T" are known. The equation takes the form:

$$A_1 = \frac{k}{e^{-\frac{E_a}{RT}}}$$

Alternatively, the pre-exponential factor may be found graphically by finding the intercept of the Arrhenius plot (plotting ln(k) versus $\frac{1}{T}$). The natural logarithmic base is then raised to the exponent of the y-intercept to find the pre-exponential factor "A_1".

$$A_1 = e^{(y-intercept)} \quad (4)$$

Equation 4: Pre-exponential factor from Arrhenius plot equation

3.1.2 Avrami equation

The Avrami equation is used to calculate the fraction of reacted vs. unreacted material. The value of "k" which was previously found for each time interval is inserted into the equation. The value of "n" is found experimentally by fitting the modelled temperature curve to the measured curve.

$$f = 1 - e^{(-(kt)^n)} \quad (5)$$

Equation 5: Avrami equation

f = fraction of reacted material [unitless]

k = reaction constant [$\frac{1}{h}$]

t = time [h]

n = exponential factor [no unit]

The Avrami equation predicts the progression of reactions. The amount each reaction proceeds in a one hour interval is multiplied by the expected enthalpy release of the complete reaction and the mass of the reactive component (alite, belite, aluminate, ferrite).

3.1.3 Hess's Law

Hess's law is used to find the total enthalpy change in a system in Joules

$$\Delta H_{Total} = \sum \Delta H \quad (6)$$

Equation 6: Hess's law

3.1.4 Rate of heat flow

The rate of heat flow is used to calculate the amount of energy transferred through a medium to the outside environment. In the case study, this is the heat flow out through the EPS wall in the normal direction. The heat flow is modelled once per hour and is

based on an earlier calculation of concrete temperature. The system is assumed to be in a steady state, however in reality; temperature fluctuations exist within each one-hour interval both in concrete and in the environment.

$$\frac{Q}{\Delta t} = -\lambda A \frac{\Delta T}{\Delta x} \quad (7)$$

Equation 7: Heat flow rate

Q = amount of heat transferred [J]

t = time [h]

λ = Thermal conductivity [$\frac{W}{m \times K}$]

ΔT = temperature difference between hot and cold side [K]

Δx = material thickness [m]

3.2 Heat transfer

The heat transfer equation is used to calculate the heating of the concrete due to the exothermicity of reactions.

$$Q = mc_p \Delta T \quad (8)$$

Equation 8: Heat Transfer (Murugan, 2014, p. 66)

The total value of Q is found by adding the reaction enthalpies of all the hydration reaction reactions in a one-hour period and by subtracting the heat loss to the environment. The mass value is the total mass of concrete, including both reactive and non-reactive components.

3.3 Nudura EPS Specifications

The mathematical model is constructed based on the reaction rates of the constituents of the Portland cement, taking into consideration the environmental considerations and the insulation provided by the EPS foam. The Nudura EPS forms have a density of 21.6

[kg/m^3 and a thermal conductivity (U-value of 0,537 [W/m^2·K]. (Nudura, 2021). The total thermal conductance of the EPS and concrete assembly must not exceed 0.24 [W/m^2·K].

The thickness of the Nudura EPS forms is 67mm and the inner core width selected for the study is 8" (203mm). For applications where less insulation or structural strength is required, a 6" (152mm) core width may be used. A standard Nudura block is 96" (2438mm) long and 18" (457mm) tall.

Figure 6: Standard Nudura EPS block (Nudura, 2021)

The total volume of the core can be calculated as:

$$V = l \times w \times h$$

$$V = 2{,}438m \times 0{,}2030m \times 0{,}4570m$$

$$V = 0{,}2262m^3$$

The block is fitted with polypropylene (PP) hinges that hold the inside and outside EPS at a constant distance. The PP hinges also act as a fastening point for deformed steel reinforcement bars and wall support systems used during construction. The compressive strength of a block is 103,4kPa and flexural strength is 241,3kPa (Nudura, 2019). Horizontal steel rebar is placed in the built-in slots in hinges. Vertical rebar is inserted into openings. Commonly rebar with diameters of 8mm, 10mm or 12mm is used depending on the required flexural and compressive strength of the wall.

The Nudura EPS form has a reversible interlocking system that allows for easy connection of blocks vertically. The interlocking system creates an airtight seal. During construction, the walls are supported by an adjustable alignment system, which also acts as a scaffolding support. The alignment system keeps a wall rigid during concrete pouring and allows for straightening after the concrete core is filled.

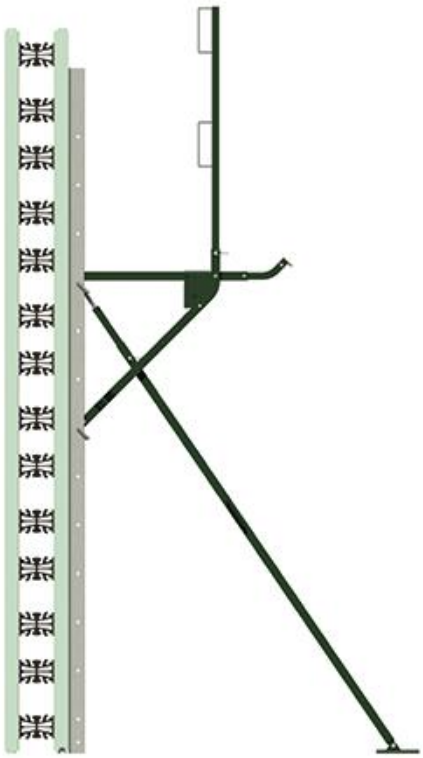

Figure 7: Nudura alignment system (Nudura, 2021)

Concrete is poured using a concrete pump, which feeds concrete through a hose, attached to a robotic, remote-controlled arm called a boom. The concrete is pumped into the EPS form and vibrated to ensure homogeneity of the particle size distribution of the mix. Vibrating the concrete also provides heat through friction.

3.4 Smartrock sensor

The Smartrock 2 sensor is made by Giatec scientific and is connected by Bluetooth to a smartphone app, where the data can be viewed and exported as a .csv file. The sensor measures the internal temperature. The sensor is placed in the cavity of the EPS form and is securely tied to reinforcement steel bars. The sensor is small and does not significantly

impede concrete flow. In the case study, the sensor is embedded in the middle of a straight wall section, where there are no window or door openings nearby. The sensor placement is selected as such, to be able to calculate the heat flow out of the system through EPS, without needing to include heat flow up or down. The heat flow to directions other than the orthogonal direction are considered negligible. The frequency of measurements is once per hour.

Based on the temperature and time measurements, a value of the maturity is found. Maturity is a measure allowing for the prediction of the time-dependent strength development. The unit of maturity is the time-temperature factor recorded as degree-hours or degree-days and is governed by the following equation.

$$\mathrm{TTF} = \sum ((\mathrm{T}_a - \mathrm{T}_0) \times \Delta \mathrm{t}) \quad (9)$$

Equation 9: Maturity function (Minnesota Department of Transportation, 2017)

T_a = Average temperature per time interval [°C]

T_0 = Minimum temperature of reaction (0 [°C], unless otherwise specified)

Δt = Time interval [h]

A maturity calculation can be performed to estimate how the development of hydration reactions is proceeding. The relationship between the strength and maturity is given by the following equation.

$$MR = S_u e^{-(\frac{\tau}{TTF})^{\alpha}} \quad (10)$$

Equation 10: Flexural Strength (Minnesota Department of Transportation, 2017)

MR = Modulus of rupture/ Flexural strength [Pa]

S_u = Ultimate expected strength [Pa]

τ = time coefficient

α = shape coefficient

Using the maturity to estimate the strength can be used when a rough estimate is adequate. Sources of inaccuracy are the estimations of the shape and time coefficients, which vary depending on the composition of the concrete mixture and the application. The accuracy of the calculated strength can be improved by conducting destructive tensile strength test

and comparing the results. The calculated estimate of strength will yield a smoother development than occurs in concrete. At temperatures near or below zero degrees Celsius, strength development may also be slower than maturity calculations estimate for.

Figure 8: Smartrock 2 sensor (Giatec Scientific, 2021)

The sensor data can be used to check that the temperature does not reach levels that may cause thermal damage. The sensor is inserted into a wall section at a height of 2200 [mm] in a straight wall section far from window and door openings. The sensor is taped to reinforcement steel in the center of the wall. The sensor used and its placement are shown in the images below.

Figure 9: Smartrock Sensor (2)

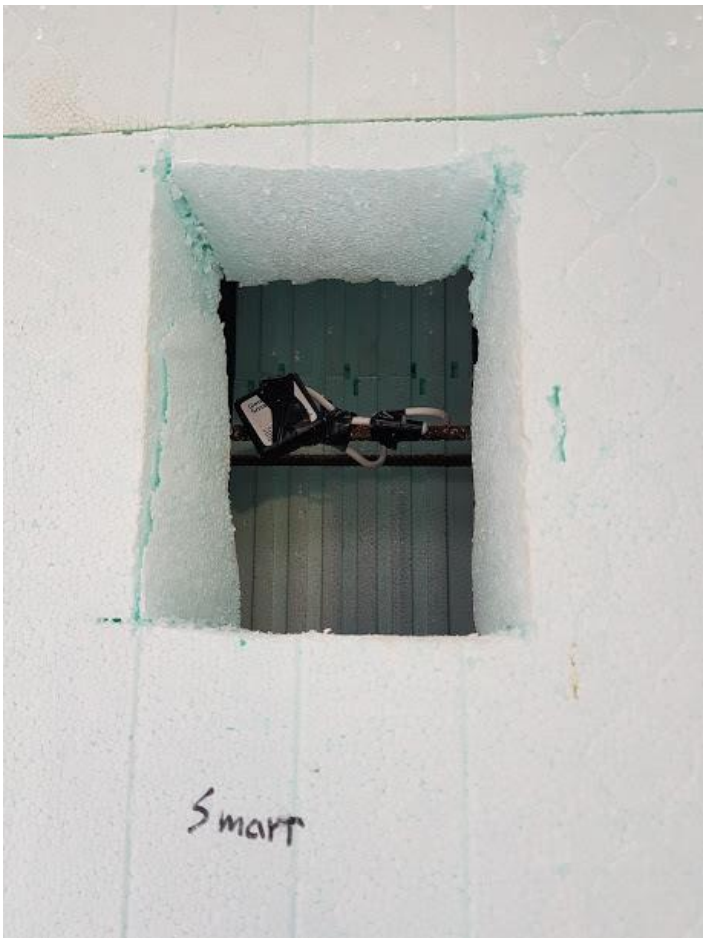

Figure 10:SmartRock sensor placement in ICF section

The temperature data received from the sensor and used as the framework for the mathematical model is presented in the graph below.

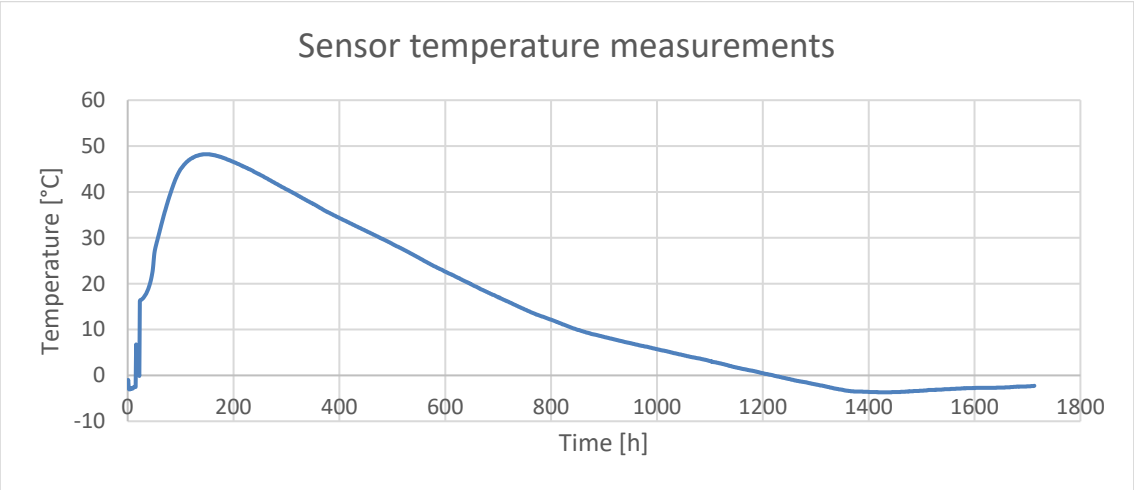

Figure 11: SmartRock temperature measurement data

The concrete is poured at t = 25 [h], where the temperature is observed to increase from values near zero to 16,2 [°C]. The values before 25 hours are neglected for the purposes of the study, as they read the temperature of the activated sensor before the concrete reaches it. The spike in temperature before reaching the temperature of 16,2 [°C] is due to small amounts of concrete hitting the sensor in the initial phases of the pour.

Concrete curing is considered safe when the temperature does not exceed 70 [°C] and does not reach below 5 [°C] during the first 48 hours of curing (Giatec Scientific, 2021). Ideal concrete curing for Type III (quick setting) cement is outlined in a study by the Portland Cement Association as 40 [°F] (4,4 [°C]), slightly lower than the optimal temperature of curing for cement types I and II (Klieger, 1958). For optimal curing, the temperature should be as stable as possible with no large increases or decreases.

3.5 Concrete

Nudura outlines the minimum allowable compressive strength of 17.25 [MPa] after 28 days and a maximum aggregate diameter of 19 [mm]. The concrete used in the case study is a high-early strength concrete. The fast setting, high-early strength concrete is selected to ensure strong exothermicity at early curing times to counteract cold outside temperatures during the pouring and to allow for the installation of ceiling concrete cavity slabs. For the modelling early strength cement composition of ASTM type III cement is used.

The density of Type III cement is measured with a pycnometer air-permeability test to equal 3066 [$\frac{kg}{m^3}$] ± 1,7 [$\frac{kg}{m^3}$].

ASTM Type III Cement composition:

Table 4: Fast setting concrete components

Compound	Content (mass %)
Ca_3S	57
Ca_2S	19
C_3A	10
C_4AF	7
Other (gypsum, MgO, $CaCO_3$, etc.)	7

Expected enthalpy release of cement constituents:

Table 5: Cement constituent enthalpies (Beaudoin & Odler, 2019)

Compound	Enthalpy [kJ/kg]
Ca_3S	520
Ca_2S	260
C_3A	1160
C_4AF	420

The concrete used in the case study is a quick-setting C25/30 concrete made by Betset. The exposure and consistency classes are outlined below.

Table 6: Case study concrete specifications

Class	Specification

Strength class	C25/30
Freeze load class	XF1
Humidity class	XC2
Consistency class	S3

4 RESULTS

A mathematical model is constructed in Microsoft Excel. To calculate a theoretical temperature of the inside of the concrete, the masses completion ratios, enthalpies, and reaction rates are modelled. Data on the strength and temperature as a unit of time is gathered from the sensor.

The temperature and reaction rates are co-dependent, and for the calculation of the reaction rate, the calculated temperature of the previous hour is used to estimate the reaction rate. A time-dependent script is built with calculations of all the variables running through a period of 28 days (672 hours).

4.1 Masses of reactants

The total masses of the concrete constituents are calculated based on the mass fraction and the total mass of the concrete.

$$Total\ mass = volume \times density \tag{11}$$

$$m = v \times \rho$$

Equation 11: Mass per volume equation

$$Total\ mass = 0{,}2262\ [m^3] \times 3066\ [\frac{kg}{m^3}]$$

$$Total\ mass = 693{,}5\ [kg]$$

The total cement content is typically between 10-15%. For the purposes of this study, a cement content of 15% is used.

$$Cement\ mass = total\ mass * cement\ ratio$$

$$Cement\ mass = 693{,}5\ [kg] * 0{,}15$$
$$Cement\ mass = 104{,}0\ [kg]$$

Multiplying the total mass by the mass proportions yields the following masses of the main reactants:

Reactant (mass ratio)	Mass [kg]
Alite (0,57)	59,29
Belite (0,19)	19,76
Aluminate (0,10)	10,40
Ferrite (0,07)	7,282
Other (0,07)	7,282

4.2 Alite reaction

The alite hydration reaction is the main heat-producing reaction in the early stages of concrete curing. In ASTM type 3 concrete, the alite content is high and the particle size is small. The main hydration peak, according to literature, occurs between t = 10-15 [h] after initiation of the reaction (Bergold, et al., 2015). During the hydration peak the rate of heat evolution reaches a maximum of between 4 and 5mW/g in isothermal conditions (Bergold, et al., 2015) (Gartner, et al., 2002) (Molèn, 2014). The pre-induction and induction periods are poorly described in the literature and will be excluded in experimental temperature change calculations.

Enthalpy of hydration = 520 $[\frac{kJ}{kg}]$ (Beaudoin & Odler, 2019). A total completion of 90% of the theoretical enthalpy is assumed.

4.2.1 Reaction rate

The reaction rate of alite dissolution and hydration is dependent on the fineness of the grinding and the temperature. The water to solid (w/s) ratio also changes the reaction rate. The temperature dependence of the alite hydration reaction is described by the Arrhenius

equation and the total completion ratio of the reaction is described by the Avrami equation.

Reaction rate k is modelled by fitting parameters to calorimeter data of existing studies.

An experimental reaction rate k is found in a 2007 study by Jeffrey J. Thomas. The values described are listed below.

Table 7: Fit parameter k values (Thomas, 2007)

Temperature [°C]	K $[\frac{1}{h}]$
10	0,04824
20	0,1060
30	0,1859
40	0,2962

The Arrhenius plot appears linear at temperatures above 20 [°C] and is modelled according to the three data points found in a 2007 study are shown in the chart above. These values are graphed in the graph below and are used to find the intercept and slope, which are used to find the pre-exponential coefficient of the Arrhenius equation.

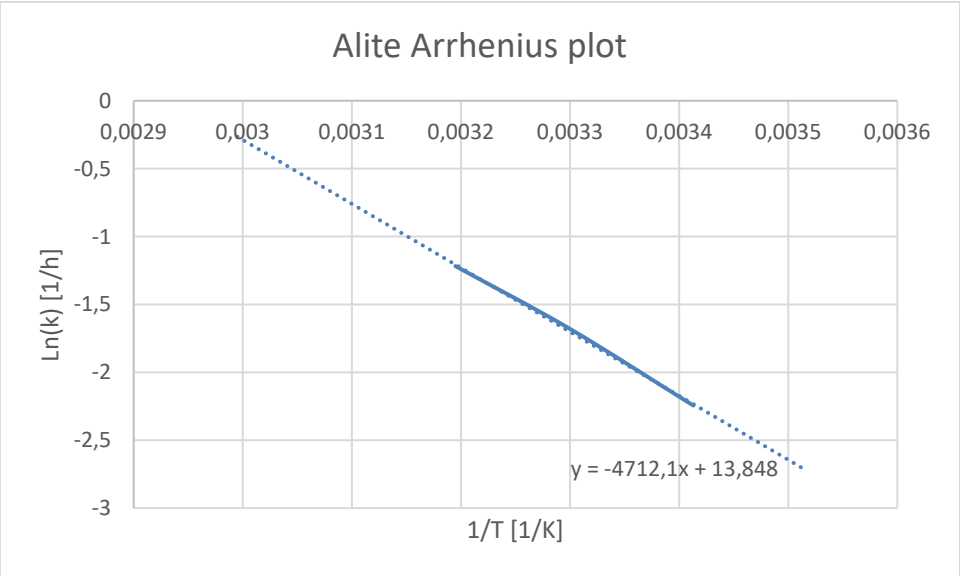

Using the trendline, by multiplying the slope of the line by the universal gas constant R (8,314 $[\frac{J}{kg \times mol}]$, can be used to estimate the activation energy of the reaction.

$$E_a = R \times slope$$

$$E_a = 8{,}314 \times (-4712{,}1)$$

$$E_a = 39180 \text{ [J]}$$

The experimental activation energy E_a is found as 39,18 $[\frac{kJ}{mol}]$, which is within the wide range of literature values (Thomas, 2007).

To find the experimental temperature dependence of the reaction rate k, the natural exponential function of y-intercept of the Arrhenius plot is used. The governing value for the temperature dependence is the pre-exponential factor A.

$$A = e^{(intercept)}$$

$$A = e^{(13{,}85)}$$

$$A = 1035100$$

4.2.2 Avrami Completion ratio

The temperature dependent k values are used to calculate the completion of the alite hydration reaction for a given time. The main hydration peak occurs early in the reaction and continues slowly for weeks or months. The change in the completion ratio per unit time (hours), the total mass of the alite in the concrete and the enthalpy change in the complete reaction can be used to estimate the amount of heat released per time interval.

$$f = 1 - e^{(-kt^n)}$$

The exponent n is variable depending on the ratio of nucleation and diffusion rates. The factor n is the exponentiality of the equation is a variable that is changed to fit the measured temperature of the concrete and is adjusted to match previous calorimeter studies of the hypothetical rate of completion. As most calorimeter studies are completed isothermally at room temperature (approximately 20°C), the case study completion is to be

expected to be faster, since the temperature in the concrete at the most important alite hydration periods is mainly above room temperature The value for k is the temperature dependent reaction constant described by the Arrhenius equation.

Determining the enthalpy release per time interval is estimated by using the progression of the Avrami completion per time interval [h]. An exponent of $\frac{1}{15}$ is found to fit the measured sensor data, as well as experimental calorimetry studies of completion rate. The calculated completion ratio as a function of time is plotted below.

Figure 12: Alite Avrami completion ratio

4.2.3 Alite enthalpy

The heat released by the alite hydration is calculated by multiplying the mass of alite in the concrete by the progression (%) of the reaction in a one-hour interval and the total expected heat release of the complete reaction. This equation is based on the progression of the reaction found with the Avrami equation for one hour, which in turn is based on the temperature dependent reaction rate constant "k" found by solving the Arrhenius equation.

$$Q = \frac{\Delta H}{t} = m_{alite}[kg] \times progression\ [\%] \times total\ enthalpy[\frac{J}{g}]$$

$$Q = \frac{\Delta H\ [J]}{t[\ h]} = 395{,}3\ [\text{kg}] \times progression\ [\%] \times 520\ [\frac{J}{g}]$$

Using the progression of the reaction per one hour interval, the total heat release can be estimated. The results of the alite hydration heat are outlined below.

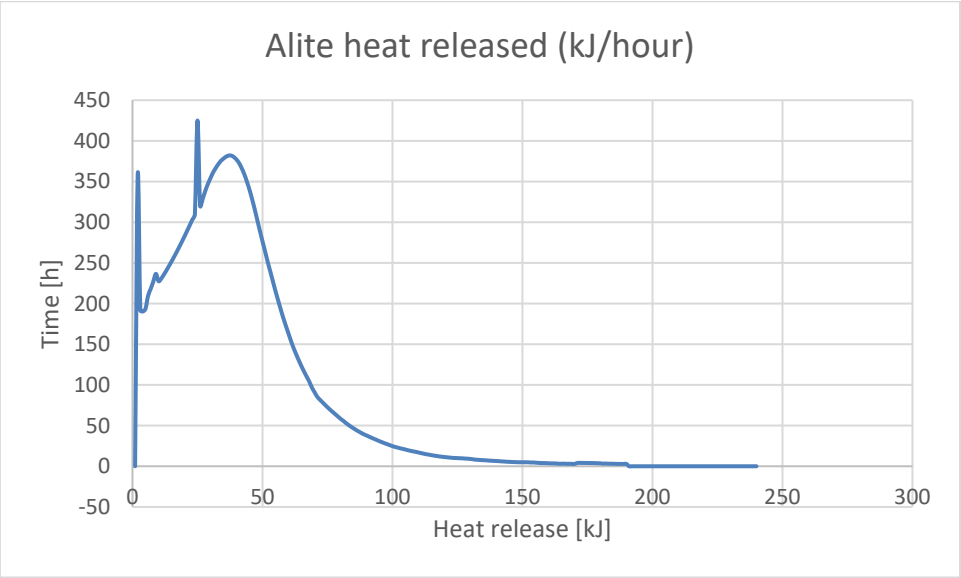

Figure 13: Alite heat release rate

Notable features of the graph are the initial hydration peak, as well as the acceleration and deceleration periods. A larger peak in the hydration rate is also seen when the rapid reaction of aluminate with water is initiated, after the initial reaction with gypsum is complete. This releases a large amount of heat into the system in a short period of time. The rate of heat release is the highest during the acceleration period and reaches a maximum between 19 and 23 hours after initiation. Literature values list the main alite hydration peak happening between 14 and 20 hours. The main hydration peak according to literature reaches a maximum of between 4 and 5 $[\frac{mW}{g}]$ (Okiemute, 2016). Converting from [mW] to [J] yields 14,4 $[\frac{J}{g}]$. Calculating the hydration heat rate for the experimental alite hydration is done by:

$$Heat\ rate = \frac{reaction\ completion\ step \times total\ heat\ of\ hydration}{3600\ [seconds]}$$

4.3 Belite reaction

The belite hydration reaction progresses slowly with calorimetry studies suggesting that the hydration degree reaches around 40% at 1000 hours (Gartner, et al., 2011). The stages of hydration are similar to those of alite, however they happen much slower.

4.3.1 Hydration rate

To find the temperature dependent reaction rate k of belite, isothermal calorimetry data from a 2017 study is used. In the study, different samples of belite are used with different calcination temperatures during production. For this thesis, the calorimetry heat of hydration data of 800[°C] calcination temperature of belite is used (Thomas, et al., 2017). The solution to the Arrhenius equation is extracted from calorimeter data at different temperatures. In the study, the temperature is varied between two values and for the purpose of the thesis, the mean values are used. The heat of hydration at 100 hours is studied. At 100 hours, the belite hydration reaction is in the acceleration stage.

Table 8: Belite heat of reaction (Thomas, et al., 2017)

Heat rate [$\frac{\mu W}{g}$]	Temperature [°C]
91	40
134	50

Using the heat rate and the temperature, an Arrhenius plot (ln(k) vs. 1/T) can be created and the slope determined. The theoretical activation energy is 32 [$\frac{kJ}{mol}$].

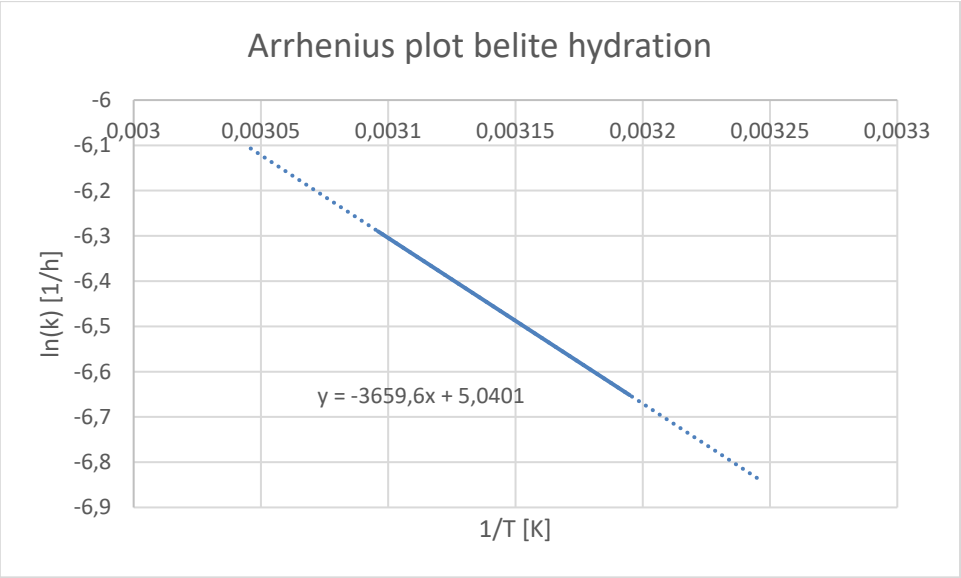

Figure 14: Belite hydration Arrhenius plot

The slope of the line corresponds to the activation energy divided by the gas constant R. Therefore, the experimental activation energy is:

$$E_a = slope \times R$$

$$E_a = -3659{,}6 \times 8{,}314$$

$$E_a = 30430 \frac{J}{mol}$$

To find the values of A, The y-intercept of the line is used. The y-intercept corresponds to the value of ln(A).

$$5{,}0401 = \ln(A)$$

$$A = 154{,}5$$

Using the value of "k" found using the Arrhenius equation, the Avrami completion ratio can be calculated. Based on the completion within a time interval (one hour) and the enthalpy of the complete hydration reaction of belite, the total heat released due to the belite hydration in any one-hour interval can be calculated.

The total heat release is calculated using:

$$Q = \frac{\Delta H}{t} = m_{belite}[kg] \times progression\ [\%] \times total\ enthalpy[\frac{J}{g}]$$

The hydration rate is outlined in the graph below.

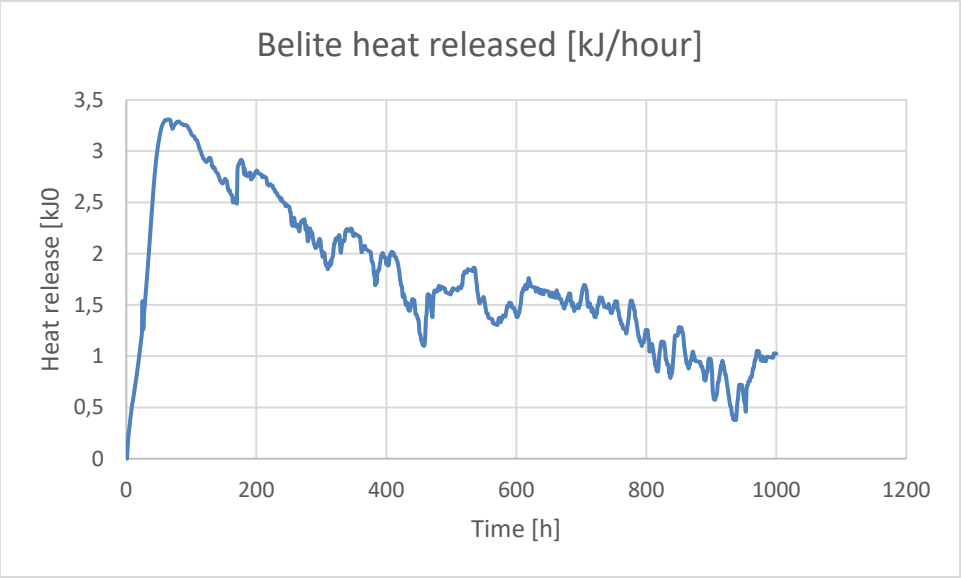

Notably, the reaction grows steadily for approximately the first 100 hours, after which the reaction rate decreases. The graph also shows the changes in the reaction rate due to heat released to the outside environment.

4.4 Aluminate Hydration

For calculation of the reaction rate of aluminate, a gypsum content of 30% is assumed, which will cause a linear increase in the reaction rate, after which a sharp peak follows, releasing most of the heat of hydration. Subsequent reactions with iron are outlined in the next section.

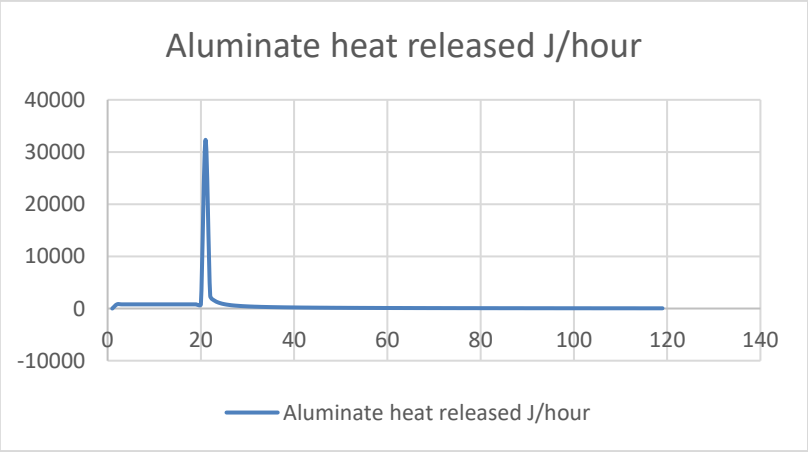

4.5 Ferrite Hydration

The ferrite hydration reaction in early stages follows the gypsum-controlled reaction rate of aluminate, and the ferrite and gypsum reaction heat release is determined using the reaction rate of aluminate and gypsum.

4.6 Total hydration heat

The total heat generated by hydration reactions is shown below. The visible peaks in the heat release are due to the initial breakdown reactions of alite, and the fast hydration reactions of aluminate and ferrite after the breakdown of the gypsum content. This is estimated to happen at 26 hours of curing. The model could further be improved by calculating the relationship between the gypsum-consuming reactions and the initiation of the aluminate-ferrite hydration.

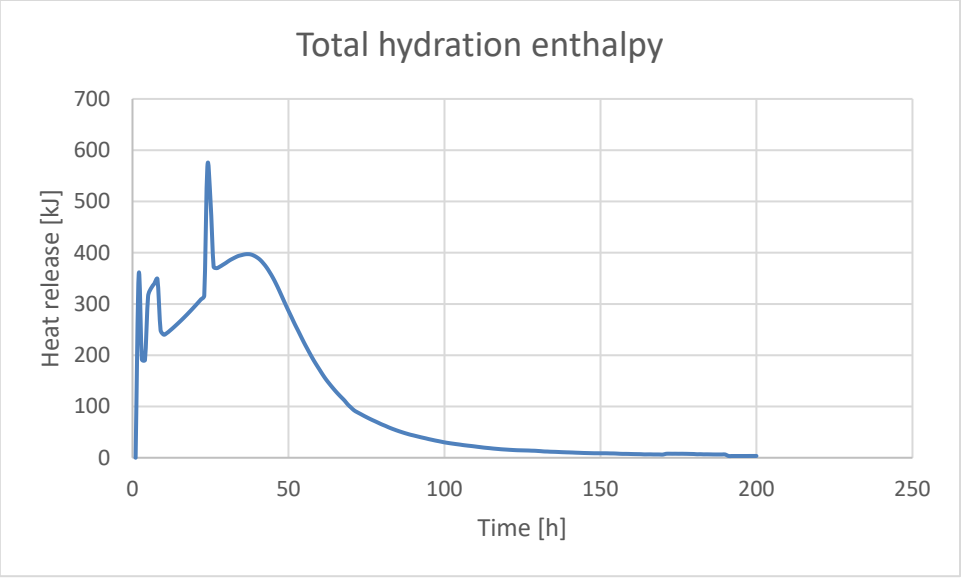

4.7 Heat flow to external environment

The heat flow to the outside environment is modelled using the heat flow rate equation. The equation is used to model the heat flow in a one-hour time interval. During each interval, the temperature of both the concrete and the environment is estimated to be in a steady state. In reality the temperatures are transient. The modelled temperatures have a resolution of one hour.

$$\frac{Q}{\Delta t} = -\lambda A \frac{\Delta T}{\Delta x}$$

The parameters used to calculate the heat flow are the thermal conductivity λ of Nudura EPS (0,036 [W/m·K]), the surface area of a block.

$$A = l \times w \tag{12}$$

Equation 12: Area equation

$$A = 2{,}438\ [m] \times 0{,}4570\ [m]$$

$$A = 1{,}114\ [m^2]$$

The temperature on both sides of the EPS. The inside temperature is the theoretical temperature gain due to the exothermicity of the hydration reactions and the outside temperature is the environmental temperature as measured by CustomWeather as listed on timeanddate.com (CustomWeather, 2021). Δx is the thickness of each EPS side (0,067 [m]).

The total heat flow out through the EPS form is multiplied by two as the heat flows through the two identical forms on each side. As a function of time, the estimated heat flow is shown in the graph below. The heat loss is considered one dimensional and is perpendicular to the concrete. A gradient in temperatures will exist between the inside and outside surfaces of the ICF system. The temperature will be the highest in the middle of the concrete core, decreasing toward the outside surface of the EPS.

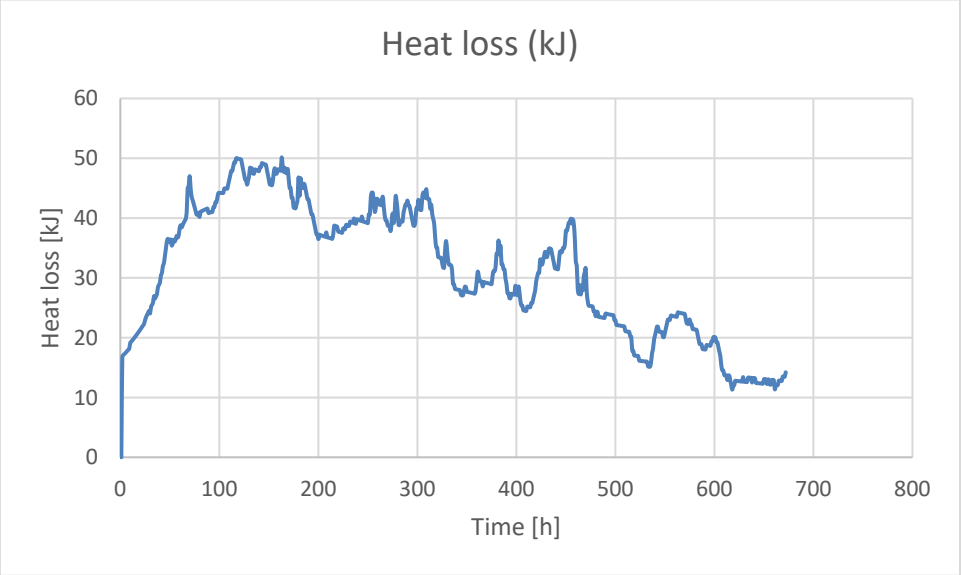

Table 9: Heat flow to environment

The initial large heat loss related to the sudden increase in the inside concrete temperature and the persisting cold outside temperatures is to be noted. The heat flow through EPS to the outside environment is directly related to the temperature difference between the core and the outside air. Differences in the flow may also be observed between days and nights as the temperature fluctuates.

4.8 Model Verification

The theoretical model is verified using data from another construction site. The secondary site was completed in early April and outside temperatures were warmer. The sensor was placed near the top surface of the concrete at a depth of 15 [cm] and therefore the heat flow up through concrete was significant and was added to the original model. The conduction up through the concrete form and out to the environment was modelled using the heat flow rate equation. A thermal conductivity of hard concrete of 1,7 $[\frac{W}{m \times K}]$ was used (Engineering ToolBox, 2003).

The same model used earlier, involving the Arrhenius and Avrami equations is used to model temperature data from a secondary site. The results are shown in the model below.

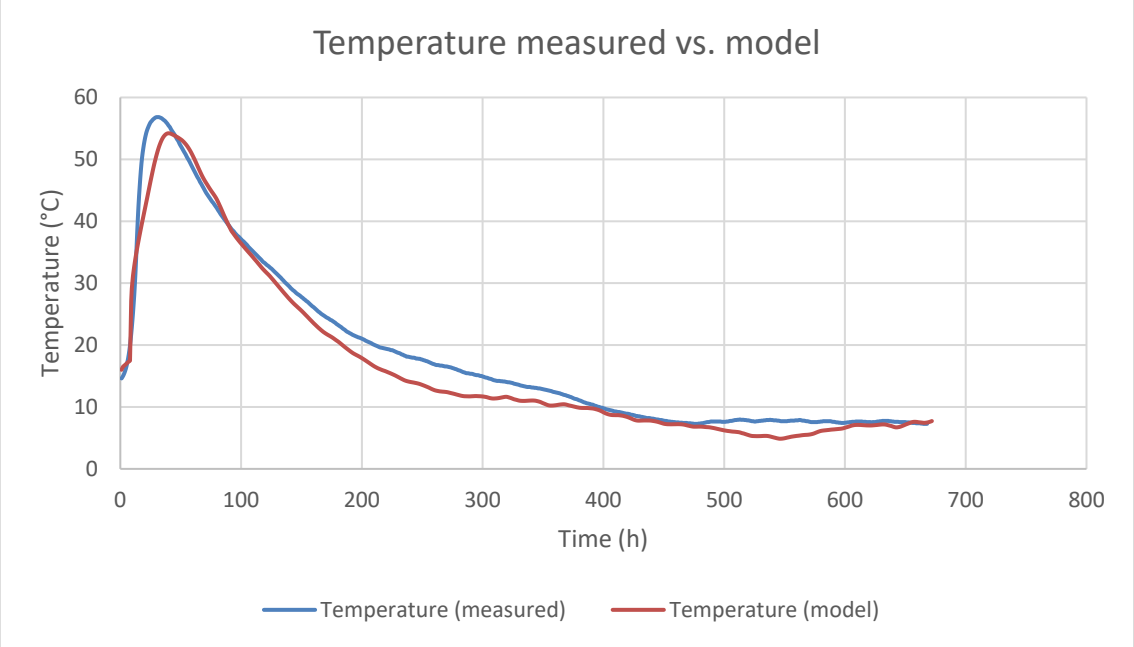

Figure 15: Temperature model verification (site two)

The error of the model and the measured values in the verification model is ±11°C at most. This occurs early in the setting of the concrete, where there are the most variables affecting the estimation. Most of the model is much more accurate. The model temperature is similar to the slope of the measured values, however the maximum temperature is reached at 41 hours of curing in the model and at 30 hours in the measurements.

The error of the experiment could be improved by tuning the exponents in the Avrami equations to change the reaction rates of the constituent clinker components. More temperature readings from various sites and temperature conditions could be used to improve the accuracy of the prediction. The most important data to be gathered is the rate of change in the temperature, especially later in the setting.

4.9 Strength

The strength development is predicted using the maturity for the first 28 days of curing. The following graph shows the measurements. The calculations are to an accuracy of ± 0,1 [MPa].

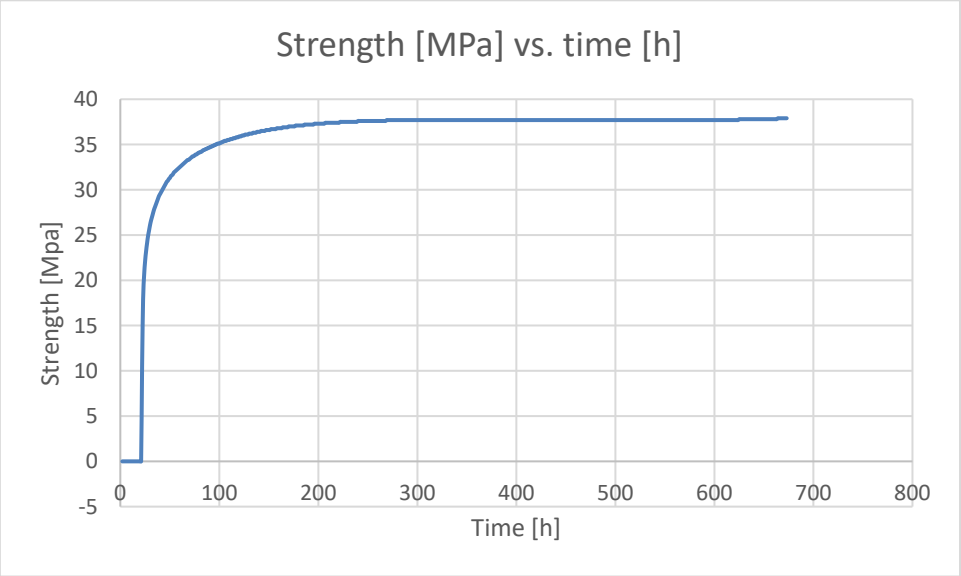

Figure 16: Strength development over time

Sensor does not provide strength measurements for the first 20 hours of curing. The strength development between 0 and 20 hours is assumed to grow exponentially to the

first measurement at 21 hours. The strength increases rapidly initially, as alite and aluminate are hydrated. The graph of the development of strength follows a similar shape to the total enthalpy release of reactions.

5 DISCUSSION

Reviewing theoretical temperature calculations, it can be stated that an estimation of the inside temperature can be modelled to an accuracy of ± 3,4 [C]° for the period of 28 days (672 hours). Several factors affect the rates of reaction of the concrete constituent elements, and it is difficult to perfectly simulate conditions. More information on the exact composition of the cement and simulation of particle interactions and void content can be used to improve the simulation. For the first case study the following graph was found comparing theoretical and experimental results:

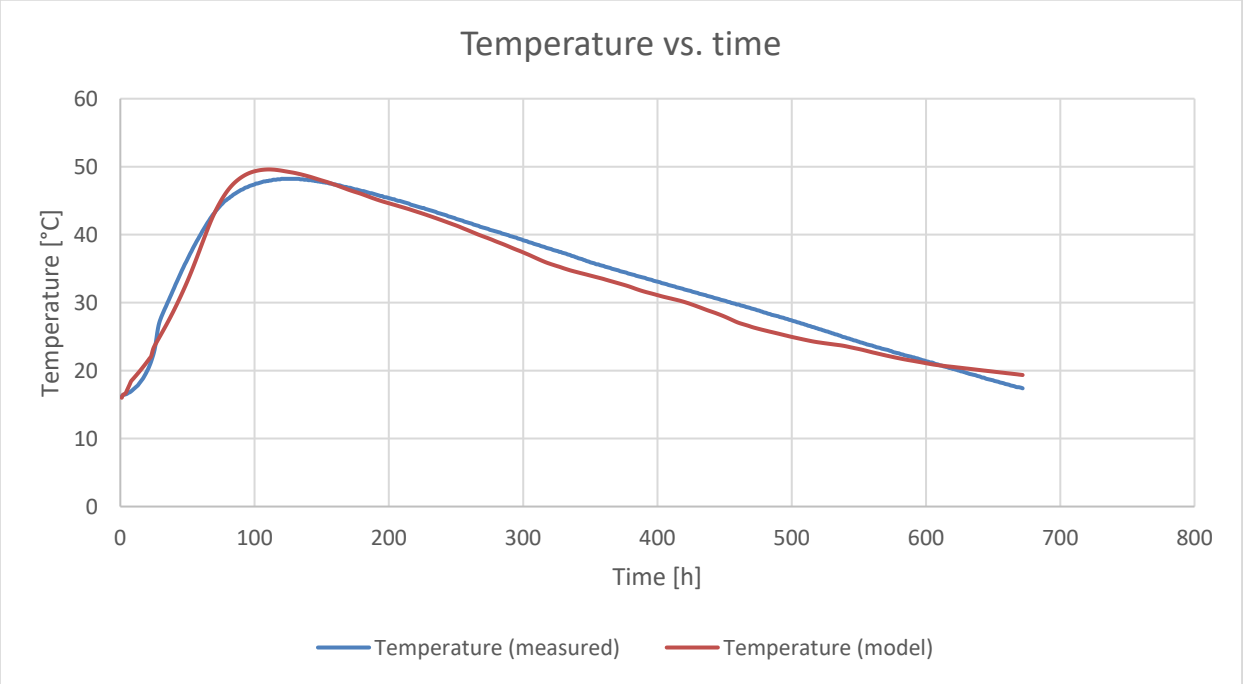

Figure 17: Temperature model

To verify the integrity of the model, data from a secondary site is included. In the second site, the sensor is at the surface of the concrete as opposed to the center of a wall far from openings as in case study 1 and its accuracy verifies the integrity of the basic components of the initial model. The Excel model created for the purposes of this thesis offers an intuitive tool where material dimensions, starting temperatures, outside temperatures and

concrete component proportions can be easily inserted to predict curing temperature as a function of time.

Due to the thermal insulation of the EPS, structural failure due to thermal shock or incomplete curing is unlikely in the bulk concrete content. In extreme outside conditions, failure of exposed concrete surfaces is possible. Inserting a theoretical outside temperature of -20 [°C] into the model for case study 2, possible incomplete curing appears possible when alite hydration rate reaches 55%, where the completion ratio appears to decrease. Additionally, when modelling a concrete surface temperature of -20 [°C], the model predicts the temperature falling below the recommended limit defined by the Portland Cement Association as 4,4 [°C] at 120 hours. According to model predictions, additional insulation should be added to cement surfaces to ensure complete curing of small amounts of alite content as well as the majority of the belite hydration reactions. Modelling for outside temperatures of – 30 [°C], an uninsulated surface reaches the critical limit of 4,4 [°C] already within 89 hours of curing, which may cause significant deterioration. Applying insulation or heating to concrete surfaces is therefore important to ensure structural integrity. ICF is efficient at stopping heat loss through wall sections, however the top surface of walls is often exposed and in extremely cold conditions it is important to cover them with adequate insulation.

The estimated strength of the concrete reaches the design strength of 30 [MPa] at 41 hours of curing, after which the strength continues to slowly increase up to 38 [MPa]. The rate of strength development is similar to the predicted completion rates of the hydration reactions of the cement compounds, showing a strong correlation to the total enthalpy release shown in the graph below.

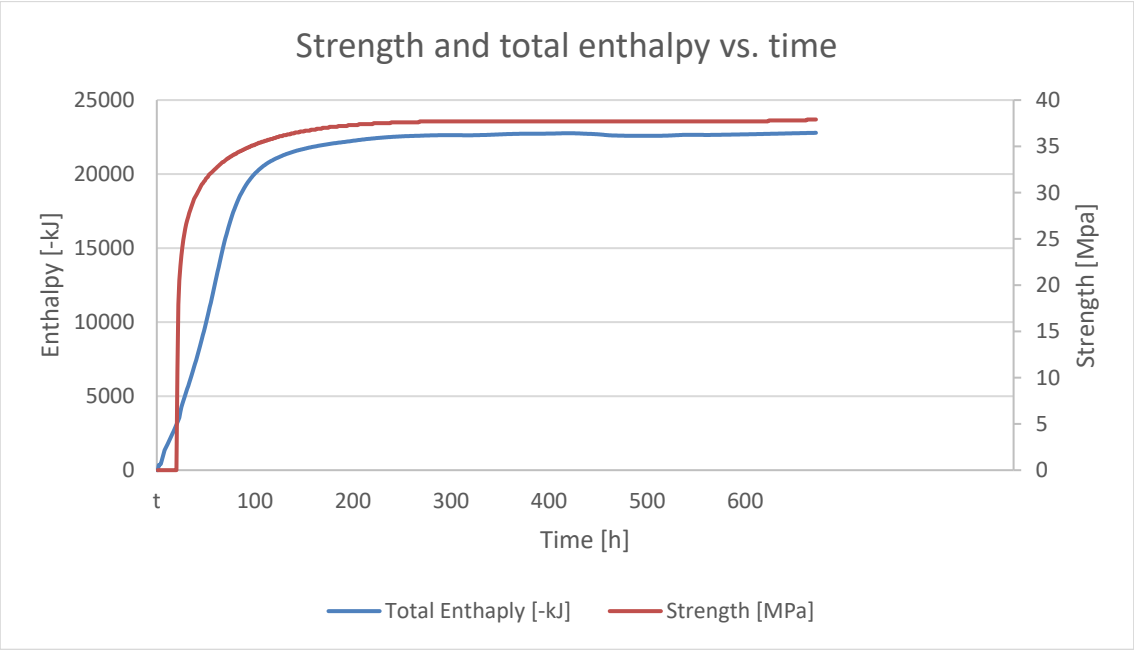

Figure 18:Strength and total enthalpy vs. time

The increase in the strength appears to happen faster than the rate of the enthalpy release. This may happen due to the early hydration reactions being able to create larger crystalline structures, as there is more available space. As hydrated crystals grow, there is less available space and new crystals are smaller, contributing less to the strength.

Concrete curing in the studied ICFs is sustainable at cold outside temperatures for sections that are not exposed to outside air. Sections that are exposed, must be insulated in extreme conditions or the structural integrity may be compromised. Most of the strength develops rapidly, as the initial alite and aluminate reactions proceed, emphasizing the importance of protecting the concrete during the early curing period. The rapid initial increase in strength shows that in bulk content of EPS insulated concrete, the curing is adequately protected from cold outside temperatures. The maturity develops rapidly, as the initial alite and aluminate reactions proceed, emphasizing the importance of protecting the concrete during the early curing period. The rapid initial increase in strength shows that in bulk content of EPS insulated concrete, the curing is adequately protected from cold outside temperatures.

In future studies additional factors such as the water content as a function of time and temperature gradients within concrete should be added. Reviewing more calorimetry studies can also provide more insight into the reaction rates of the various components and the interactions of the hydrating crystals. The literature on the curing of concrete

outside laboratory conditions can be further examined to improve the accuracy of theoretical curing rates of concrete components. More data should be collected on inside temperatures and strengths of concrete in various curing conditions and time frames in real construction projects. Future research into concrete curing can be used to improve safety of construction. The environmental impact of concrete construction can also be reduced by changing concrete compositions to such that do not require high kilning temperatures. By improving the literature on the effects of temperature on the curing of concrete, novel mixes of concrete can be engineered to fit specific requirements of cold climate concreting.

6 REFERENCES

Barron, A. R., 2010. 3 Chemical Composition of Portland Cement. In: *Portland Cement in the Energy Industry*. Houston: Rice University, pp. 7-8.

Beaudoin, J. & Odler, I., 2019. Hydration, Setting and Hardening of Portland Cement. In: P. C. Hewlett & L. Martin, eds. *Lea's Concrete Chemistry*. Oxford: Elsevier Science and Technology, pp. 157-250.

Bentz, D. P., 1997. Three-Dimensional Computer Simulation of Portland Cement Hydration and Microstructure Development. *Journal of the American Ceramic Society*, 80(1), pp. 3-21.

Bergold, S., Goetz-Neunhoeffer, F. & Neubauer, J., 2015. Mechanically activated alite: New insights into alite hydration. *Cement and Concrete Research*, Volume 76, pp. 202-211.

Berman, H. A. & Newman, E. S., 1963. Heat of Formation of Calcium Aluminate Monosulfate at 25 °C. *Journal of Research of the National Institute of Standards and Technology*, pp. 1-13.

Bishnoi, S. & Scrivener, K. L., 2009. Studying nucleation and growth kinetics of alite hydration using μic. *Cement and Concrete Research*, 39(10), pp. 849-860.

British Standards Institution, 2011. *BS EN 197-1:2011*. [Online] Available at: http://106.38.59.21:8080/userfiles/d46365fdde004ea0a5da5d9701142815/files/teckSolution/2019/10/EN%20197-1-2011_3750.pdf
[Accessed 11 March 2021].

Carlson, E. T., 1964. Action of Water on Calcium Aluminoferrites. *Journal of Research of the National Institute of Standards and Technology*, p. 453–463.

Carraher, C. E. J., 2017. *Introduction to Polymer Chemistry*. 4th ed. Boca Raton: Taylor & Francis Group.

Christensen, N. H. & Smidth, F., 1979. Burnability of cement raw mixes at 1400°C II the effect of the fineness. *Cement and Concrete Research*, 9(3), pp. 285-294.

Colorado State University, Heat transfer mechanisms. *Review of Heat Transfer.* [Online] Available at: https://www.engr.colostate.edu/~allan/heat_trans/page4/page4f.html#:~:text=Convection%20heat%20transfer%20is%20energy,fluid%20motion%20along%20the%20surface.&text=The%20temperature%20difference%20usually%20occurs,adjacent%20to%20the%20solid%20surface.
[Accessed 12 6 2021].

CustomWeather, 2021. *timeanddate.* [Online] Available at: https://www.timeanddate.com/weather/finland/helsinki/historic

Del Strother, P., 2019. Manufacture of Portland Cement. In: P. C. Hewlett & M. Liska, eds. *Lea's Chemistry of Cement and Concrete.* Oxford: Butterworth-Heinemann, pp. 31-56.

Dunuweera, S. P. & Rajapakse, R. M. G., 2018. Cement Types, Composition, Uses and Advantages of Nanocement, Environmental Impact on Cement Production, and Possible Solutions. *Advances in Materials Science and Engineering* , 1 August, pp. 1-11.

Engineering ToolBox, 2003. *Thermal Conductivity - selected Materials and Gases.* [Online]
Available at: https://www.engineeringtoolbox.com/thermal-conductivity-d_429.html [Accessed 10 August 2021].

EPS Recycling International, 2019. *EPS Recycling.* [Online] Available at: https://epsrecycling.org/eps-recycling

Gagg, C. R., 2014. Cement and concrete as an engineering material: An historic appraisal and case study analysis. *Engineering Failure Analysis*, Volume 40, pp. 114-140.

Gartner, E. M. & Jennings, H. M., 1987. Thermodynamics of Calcium Silicate Hydrates and Their Solutions. *Journal of American Chemical Society*, 70(10), pp. 743-749.

Gartner, E. M. et al., 2011. *Hydration of a Belite-CalciumSulfoaluminate-Ferrite cement: AetherTM.* Madrid, 13th International Congress on the Chemistry of Cement.

Gartner, E. M., Young, J. F., Dammidot, D. A. & Jawed, I., 2002. Hydration of Portland Cement. In: J. Bensted & P. Barnes, eds. *Structure and Performance of Cements.* New York: Taylor & francis, pp. 57-114.

Giatec Scientific, 2021. *Giatec.* [Online] Available at: https://www.giatecscientific.com/products/concrete-sensors/smartrock2-concrete-sensor/

Glasser, F. P., 2003. The Burning of Portland Cement. In: P. C. Hewlett, ed. *Lea's Chemistry of Cement and Concrete.* Oxford: Elsevier, pp. 233-236.

Gromicko, N. & Shepard, K., n.d. *The History of Concrete,* Boulder: International Association of Home Inspectors.

Haldar, S. K., 2014. *Introduction to Mineralogy and Petrology*. Oxford: Elsevier.

Hanson Heidelberg Cement Group, 2020. *Types of Cement Used In The Construction Industry.* [Online] Available at: https://www.hanson.my/en/types-cement-construction-industry

Harrison, T. A. & O, B., 2007. *How to specify concrete for civil.* [Online] Available at: file:///C:/Users/ThinkPad/Downloads/HowTo_BS8500CivilEng_May20.pdf [Accessed 15 March 2021].

Jewell, R. et al., 2015. Fabrication and Testing of Low-Energy Calcium Sulfoaluminate-Belite Cements that Utilize Fluidized Bed Combustion By-Products. *Coal Combustion and Gasification Products,* pp. 9-18.

Klieger, P., 1958. Effect of Mixing and Curing temperature on Concrete Strength. *Portland Cement Association bulletin 103.*

Kumara, A., Bishnoib, S. & Scrivenera, K. L., 2012. Modelling early age hydration kinetics of alite. *Cement and Concrete Research,* 42(7), pp. 903-918.

Manzano, H., Dolado, J. & Ayuela, A., 2009. Elastic properties of the main species present in Portland cement pastes. *Acta Materialia,* pp. 1666-1674.

Minerals Education Coalition, 2021. *Minerals Database.* [Online] Available at: https://mineralseducationcoalition.org/minerals-database/limestone/#:~:text=Most%20limestone%20and%20dolomite%20are,scale%20production%20by%20underground%20mining.&text=Underground%20Limestone%20Mining%3A,hauling%2C%20scaling%20and%20roof%20bolting.
[Accessed 16 May 2021].

Minnesota Department of Transportation, 2017. *Estimating Concrete Strength by the Maturity Method.* [Online] Available at: https://www.dot.state.mn.us/materials/concretedocs/MaturityMethodProcedure.pdf
[Accessed 1 11 2021].

Molèn, M., 2014. *Early hydration of Portland Cement,* Gothenburg: Institutionen för Kemi- och Bioteknik Chalmers Tekniska Högskola.

Molero, M. et al., 2012. Evaluation of freeze-thaw damage in concrete by ultrasonic imaging. *NDT & E International*, pp. 86-94.

Mortimer, M. & Taylor, P., 2002. *Chemical Kinetics and Mechanism.* Cambridge: Royal Society of Chemistry.

Murugan, S., 2014. *Engineering Thermomechanics.* Oxford: Alpha Science International Ltd..

Möschner, G. et al., 2008. Solubility of Fe–ettringite (Ca6[Fe(OH)6]2(SO4)3 · 26H2O). *Geochimica et Cosmochimica Acta,* 1 January, 72(1), pp. 1-18.

Neville, A., 2011. *Properties of Concrete.* Essex: Pearson.

Nicoleaua, L. & A., N., 2016. A new view on the kinetics of tricalcium silicate hydration. *Cement and Concrete Research,* Volume 86, pp. 1-11.

Nmai, C., Bury, M. & Daczko, J., 2018. *SHRINKAGE OF CONCRETE: MINIMIZING/ELIMINATING THE POTENTIAL FOR CRACKING,* s.l.: Tilt-Up Concrete Association.

Nobre, J. et al., 2020. Magnesia (MgO) Production and Characterization, and Its Influence on the Performance of Cementitious Materials: A Review. *Materials*, 23 October .

Nudura, 2019. *Nudura.com.* [Online] Available at: https://www.nudura.com/media/3526/nudura_10_part_specification.pdf?sfvrsn=0

Nudura, 2021. *Nudura.com.* [Online] Available at: https://www.nudura.com/media/1965/1_0_introduction_to_nudura_insulated_concrete_forms.pdf

Nudura, 2021. *Nudura.com.* [Online] Available at: https://www.nudura.com/products/nudura-icf-series/alignment-system/

Odler, I., 2003. Hydration, Setting and Hardening of Portland Cement. In: P. C. Hewlett, ed. *Lea's Chemistry of Cement and Concrete.* Oxford: Elsevier, pp. 241-289.

Okiemute, O., 2016. *Influence of Slag Composition and Temperature on the Hydration and Performance of Slag Blends in Chloride Environments*, Leeds: The University of Leeds School of Civil Engineering.

Omnexus, n.d. *Expanded Polystyrene (EPS): Ultimate Guide on Foam Insulation Material.* [Online] Available at: https://omnexus.specialchem.com/selection-guide/expanded-polystyrene-eps-foam-insulation

Paine, K. A., 2019. Physicochemical and Mechanical Properties of Portland Cements. In: *Lea's Chemistry of Concrete and Cement.* Oxford: Elsevier, pp. 285-339.

Paulini, P., 1990. Reaction Mechanisms of Concrete Admixtures. *Cement and Concrete Research*, Volume 20, pp. 910-918.

Pellenq, R. J.-M. & Van Damme, H., 2004. Why Does Concrete. *MRS Bulletin.*

Portland Cement Association, 2001. *Ettringite Formation and the Performance of Concrete,* s.l.: Concrete Information.

Portland Cement Association, 2019. *Cement.org.* [Online] Available at: https://www.cement.org/learn/concrete-technology/concrete-construction/cold-weather-concreting

Pustovgar, E. et al., 2016. Understanding silicate hydration from quantitative analyses of hydrating tricalcium silicates. *Nature Communications,* Volume 7.

Qi, T. et al., 2021. Predictive Hydration Model of Portland Cement and Its Main Minerals Based on Dissolution Theory and Water Diffusion Theory. *Materials,* 14(3), p. 595.

Rain Cement Limited, 2017. *Limestone crushing.* [Online] Available at: https://www.priyacement.com/products/processes2.html [Accessed 11 March 2021].

Renó, M. et al., 2017. Environmental analyze of cement production with application of wastes. *Engevista,* 19(4), pp. 916-930.

Richardson, I., 2008. The calcium silicate hydrates. *Cement and Concrete Research,* pp. 137-158.

Rodgers, L., 2018. Climate change: The massive CO2 emitter you may not know about. *BBC News,* 17 December.

Salami, T. O., 2014. *Synthesis and Working Mechanism of Humic Acid Graft Copolymer Fluid Loss Additives Suitable for Cementing High Pressure / High Temperature Oil and Gas Wells,* Munich: TECHNISCHE UNIVERSITÄT MÜNCHEN.

Schneider, M., Romer, M., Tschudin, M. & Bolio, H., 2011. Sustainable cement production—present and future. *Cement and Concrete Research,* 41(7), pp. 642-650.

Termkhajornkit, P. et al., 2014. Dependence of compressive strength on phase assemblage in cement pastes: Beyond gel–space ratio — Experimental evidence and micromechanical modeling. *Cement and Concrete Research,* Volume 56, pp. 1-11.

Thomas, J. J., 2007. A New Approach to Modeling the Nucleation and Growth Kinetics of Tricalcium Silicate Hydration. *Journal of the American Ceramic Society,* 90(10), pp. 3282-3288.

Thomas, J. J., Ghazizadeh, S. & Masoero, E., 2017. Kinetic mechanisms and activation energies for hydration of standard and highly reactive forms of β-dicalcium silicate (C2S). *Cement and Concrete Research,* Volume 100, pp. 322-328.

Tradeship Publications Ltd, 2019. *The Global Cement Report™ - 13th Edition,* s.l.: Tradeship Publications Ltd.

Vu, X.-D.et al., 2015. Influence of the Saturation Ratio on Concrete Behavior under Triaxial Compressive Loading. *Science and Technology of Nuclear Installations.*

Won, J.-Y., Lee, S.-H., Park, T.-W. & Nam, K.-Y., 2016. Basic applicability of an insulated gang form for concrete building construction in cold weather. *Construction and Building Materials,* Volume 125, pp. 458-464.

Yucel, K. T., Basyigit, C. & Ozel, C., 2003. Thermal Insulation Properties of Expanded Polystyrene as Construction and Insulating Materials.